INTERNATIONAL ATOMIC ENERGY AGENCY
UNITED NATIONS EDUCATIONAL, SCIENTIFIC AND CULTURAL ORGANIZATION

INTERNATIONAL CENTRE FOR THEORETICAL PHYSICS
34100 TRIESTE (ITALY) · P.O.B. 586 · MIRAMARE · STRADA COSTIERA 11 · TELEPHONE: 2240-1
CABLE: CENTRATOM · TELEX 460392-1

SMR/291 - 53

SPRING COLLEGE IN CONDENSED MATTER
ON
"THE INTERACTION OF ATOMS & MOLECULES WITH SOLID SURFACES"
(25 April - 17 June 1988)

GROWTH PROCESSES AT SURFACES

M. DJAFARI-ROUHANI
CNRS/LAAS
7, Av. du Colonel Roche
31077 Toulouse
France

CHAPTER I

THERMODYNAMIC MODELS

Introduction and historical survey

Thin films are of interest from many different points of view. For a long time they have been technologically important in optical coatings, corrosion protection and semiconductor devices. Many of these applications involve increasingly complex and sophisticated growth processes to produce devices such as 'heterojunction lasers' or 'multiple quantum well structures'. Thin films are also important within physical science itself in exploring differences between three-dimensional and (quasi-)two-dimensional states of matter: the decrease in conductivity of thin metal films, the variation in thermodynamic properties, or chemical reactivity, as a function of film thickness are examples. Often thin films are important in arrangements for experiments on other topics, such as absorbing x-rays or polarising neutrons.

Man made synthetic structures involving epitaxially grown thin films of one or more compound semiconductors have been finding an increasingly important role in semiconductor device technology.[1] Remarkable advances have been made over the past decade in the realization of a variety of such structures involving III–V, II–VI and IV–VI compound semiconductors, as well as combinations of semiconductors with dielectrics and metals.[1]

Because of the necessity of using single crystal material for the operation of semiconductor devices the idea of producing single crystal thin films is of obvious interest in the field of solid state electronics, and it was the advent of solid state active devices which changed the study of the growth of oriented thin films from an academic pursuit to one of considerable technological importance. Until 1960 single crystal material (mainly Ge and Si) for transistor fabrication was produced by growth from the melt and doping impurities were introduced by alloy processes,

The major part of this progress has come about primarily due to the advent of, and refinements in, two vapour phase growth techniques – Molecular Beam Epitaxy (MBE)[2] and Metal–Organic Chemical Vapour Deposition (MOCVD).[3] The underlying motivation has been the remarkably altered and potentially useful electronic and optical properties of electrons, holes and light arising from their confinement in a quasi–two dimensional environment in the ultrathin films (thickness less than the particle deBroglie wavelength).[4] However confinement of the particles in such ultra thin layers (typically 10–200°A) places stringent requirements on the atomic level structural and chemical perfection of the films and their interfaces involved. At the same time, spatial control of the abruptness (in the growth direction) and uniformity (in the planes normal to the growth direction) of dopant distribution becomes equally significant in realizing the potential electrical and optical properties of carriers and light in such structures. Both MBE and MOCVD have been shown to meet these stringent requirements for the growth of III–V compound semiconductors although differences between materials and structures produced by these techniques also remain.

MBE is an ultra-high vacuum (UHV) vapour phase deposition technique which, as practiced hitherto for growth of III–V semiconductors, involves the group III vapour in atomic form while the group V vapour is either in diatomic or tetratomic molecular form. It thus offers an ideal test system for the historical notions of crystal growth and the models and theories advanced.[16] In this context it is important to recognize that the genesis of the atomistic notions and theories of crystal growth from the vapour phase lies predominantly in models representing growth of elemental solids from atomic vapour. Consequently, it is primarily the relative role of the kinetic processes of surface migration and evaporation which has been at the heart of such models, as well as the concepts, terminology and mechanisms of growth arising from them. By contrast, a majority of crystal growth from the vapour phase, particularly of compounds, involves at least one species in molecular form. This feature introduces surface chemical reactions involving dissociation of the molecule as an integral kinetic step in the growth process. MBE of III–V semiconductors thus represent an ideal test system for the larger category of vapour phase growth since it embodies the essential physics and chemistry of crystal growth involving surface migration, evaporation and dissociative molecular reactions.

The technique of producing thin films by means of a chemical reaction at a heated substrate surface has become of great importance in semiconductor technology. The major reasons for this may be summarized as follows:

(i) Growth can be obtained at temperatures much lower than the melting point, so that problems of extraneous contamination are lessened and impurity diffusion rates within the growing film minimized.
(ii) Excellent control of layer thickness can be achieved.
(iii) Doping elements can be added in a precisely controlled manner over a very wide concentration range (10^{14}–10^{21} atoms cm^{-3}).
(iv) Material of high crystallographic perfection can be grown simply without the use of UHV techniques.

basic criteria must be met: reactive species must be transported at appropriate partial pressures to the substrate surface, which must be heated to a sufficient temperature to initiate a heterogeneous reaction. One product of this reaction must be the material of the film, and any other products must be sufficiently volatile to be removed in the gas stream.

CRYSTAL GROWTH MODES

In this introduction the three modes of crystal growth which are thought to occur on surfaces in the absence of surface defects and interdiffusion are described.

It is generally accepted that there are three possible modes of crystal growth on surfaces, which are illustrated schematically in figure 1, following Bauer (1958). In the island, or Volmer–Weber mode (figure 1(*a*)), small clusters are nucleated directly on the substrate surface and then grow into islands of the condensed phase. This happens when the atoms (or molecules) of the deposit are more strongly bound to each other than to the substrate. This mode is displayed by many systems of metals growing on insulators, including many metals on alkali halides, graphite and other layer compounds such as mica.

The layer, or Frank–van der Merwe mode (figure 1(*c*)), displays the opposite characteristics. Because the atoms are more strongly bound to the substrate than to each other, the first atoms to condense form a complete monolayer on the surface, which becomes covered with a somewhat less tightly bound second layer. Providing the decrease in binding is monotonic, toward the value for a bulk crystal of the deposit, the layer growth mode is obtained. This growth mode is observed in the case of adsorbed gases, such as several rare gases on graphite and on several metals, in some metal–metal systems, and in semiconductor growth on semiconductors.

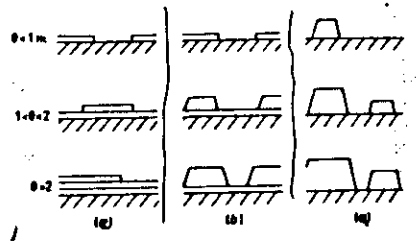

Figure 1. Schematic representation of the three crystal growth modes: (*a*) island or Volmer–Weber, (*b*) layer plus island or Stranski–Krastanov, (*c*) layer or Frank–van der Merwe mode. θ represents the coverage in monolayers (ML).

The layer plus island, or Stranski–Krastanov, growth mode (figure 1(*b*)) is an interesting intermediate case. After forming the first monolayer (ML), or a few ML, subsequent layer growth is unfavourable and islands are formed on top of this 'intermediate' layer. There are many possible reasons for this mode to occur, and almost any factor which disturbs the monotonic decrease in binding energy, characteristic of layer growth, may be the cause. For example, the lattice parameter of, or symmetry of, or molecular orientation in, the intermediate layer may not be able to be continued into the bulk crystal of the deposit. This results in a high free energy of the deposit–intermediate-layer interface which favours subsequent island formation. As will be seen later, this growth mode is much more common than was thought just a few years ago. There are now many examples of its occurrence in metal–metal, metal–semiconductor, gas–metal and gas–layer compound systems.

These three different growth modes have their thermodynamic counterparts in three different forms of adsorption isotherms illustrated in figure 2, following Dash (1977) and Kern *et al* (1979). In island growth (figure 2(*a*)), the concentration of adsorbed atoms is often very low, due to fast re-evaporation from the weakly binding substrate, and a large positive chemical potential change ($\Delta\mu$), or supersaturation, S,

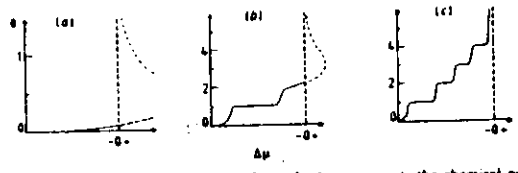

Figure 2. Adsorption isotherms corresponding to figure 1. $\Delta\mu$ represents the chemical potential of the growing deposit relative to the bulk material and θ the coverage in mL. In (*b*) two stable intermediate layers are indicated.

is needed to nucleate the deposit. The first two-dimensional (2D) layers in layer growth, however, can exist in equilibrium with the dilute three-dimensional phase at negative $\Delta\mu$ (undersaturation), as illustrated in figure 2(*c*). Here we are primarily concerned with growth from the vapour, and adsorption isotherms as illustrated are seen, for example, in rare-gas adsorption (e.g. Kr, Xe) on graphite. In the Stranski–Krastanov case, the adsorption isotherm is as illustrated in figure 2(*b*), where the $\Delta\mu = 0$ line is cut at some finite thickness, or coverage θ. Beyond this coverage, island growth is favoured thermodynamically.

The nucleation processes which occur in the deposition of epitaxial metal films on a variety of substrates have been extensively studied (see for example reviews by Pashley 1965 and Chopra 1969), but with semiconductor films they have received comparatively little attention. The reason is simply associated with the type of deposition system used. For metals, using vacuum evaporation/condensation, a high degree of control of the extent and rate of deposition is available over any time scale, including the earliest growth stages. This is not the case for chemical vapour deposition, which is widely used for the preparation of semiconductor films.

The use of chemical vapour deposition in a conventional flow reactor of the type described imposes a number of serious constraints on nucleation experiments, and such systems cannot be used to obtain quantitative nucleation data. These constraints may be summarized as follows:

(i) The length of time taken to reach steady state in the reactor is frequently longer than the period over which nucleation can be observed at realistic deposition rates. The time interval to steady state is a consequence of the comparatively low gas velocities used.

(ii) The rate-limiting step in the deposition process is often the diffusion of reactants to the substrate surface, so the arrival rate of reacting species cannot be controlled.

(iii) There is the possibility of a homogeneous component of the deposition reaction occurring in the hot gases surrounding the substrate.

(iv) The energy distribution of molecules impinging on the substrate is entirely random and uncontrolled.

The early work in which attempts were made to study nucleation in chemical vapour deposition systems was therefore entirely qualitative. Studies

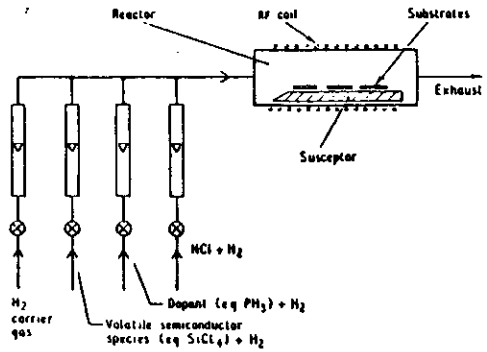

Figure 5. The essential features of a flow reactor system for chemical vapour deposition of thin films of semiconductors.

showed an apparent three dimensional nucleation process to be involved with subsequent formation of continuous, but stepped, layers by coalescence and lateral expansion. It was postulated that most of the surface topographic effects observed could be associated with surface impurities, most probably oxygen. The authors interpreted these results in terms of the relative rates of accumulation and depletion of surface contamination during deposition. The accumulation arises from residual gas–substrate interactions and oxide contamination can be removed as volatile SiO by reaction with impinging silicon atoms. For slow deposition contamination accumulates faster than it is removed so lateral growth is impeded, but at high deposition rates the inverse is true; coalescence is not impeded and growth is essentially two dimensional.

Probably the most surprising feature of the early work discussed above was the variety of growth morphologies observed by different authors. These morphologies included apparent two dimensional growth, discrete three dimensional crystallographically shaped growth centres and irregular three dimensional centres.

Because of the limitations imposed by conventional flow techniques on the study of nucleation and growth kinetics in chemical deposition systems already discussed in §3.1, Joyce and his co-workers used a molecular beam system to investigate the nucleation of autoepitaxial silicon films produced by the pyrolysis of silane. The experimental system comprised three separately pumped chambers with the silane beam first being formed from a Knudsen source, and subsequently collimated so that it impinged on the resistively heated silicon substrate in the target chamber. The base pressure in this chamber was around 10^{-10} Torr, so that it was possible to work with substrates whose surfaces could be maintained essentially clean on an atomic scale for reasonable periods. If necessary, the beam could be modulated and desorbed molecules synchronously detected with a mass spectrometer.

By using a molecular beam the flow system limitations were clearly removed. Thus (i) the beam could be stopped and started with a very short time constant using a simple shutter arrangement, (ii) there was no possibility of a homogeneous component or diffusion control of the deposition reaction and (iii) the energy of molecules reaching the substrate followed the usual shifted Boltzmann distribution from a Knudsen source.

With this system nucleation kinetic parameters were measured quantitatively in terms of the number density of nuclei, but as already shown these nuclei are only observed in the presence of surface carbon impurity. The results obtained are summarized below.

It was found that after completion of the induction period discussed in §3.2, the number density of growth centres, N_s, very rapidly reached a saturation value and then stayed constant with time until coalescence commenced.

Atomistic processes on surfaces

The individual atomic processes responsible for adsorption and crystal growth on surfaces are illustrated in figure 3. For vapour deposition from an ideal gas at pressure p, the rate of arrival R at the substrate is given by $p\,(2\pi mkT)^{-1/2}$ where m is the molecular weight, k is Boltzmann's constant and T is the source temperature; alternatively, the rate R ($m^{-2}s^{-1}$) may be assured by a molecular beam or evaporation source, or by arrival of ions from solution. This creates single atoms on the substrate (number density $n_1(t)$) on a substrate with N_0 sites per unit area, so that the single-atom concentration is (n_1/N_0). These single atoms may then diffuse over the surface until they are lost by one of several processes. These processes include re-evaporation or re-solution, nucleation of 2D or 3D clusters, capture by existing clusters, possibly dissolution into the substrate, and capture at special (defect) sites such as steps. On an ideally flat, 'inert' substrate, these last two processes would be excluded, though they may often be present in practice.

Each of these processes will be governed by characteristic times, which themselves will depend on the single-atom concentration and/or coverage. If such processes are

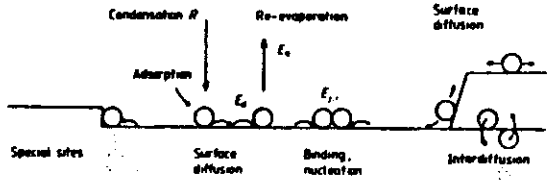

Figure 3. Schematic diagram of processes and characteristic energies in nucleation and growth on surfaces. See text for discussion.

thermally activated, then these times will in turn be controlled by activation energies and frequency factors. For example, re-evaporation at low coverage would be characterised by a time, τ_s, which could be written as $\nu^{-1}\exp(\beta E_s)$ with $\beta \simeq (kT_s)^{-1}$, T_s being the substrate temperature and ν a characteristic surface vibration frequency. Some of the important energies are indicated in figure 3. In addition to re-evaporation, there are diffusion energies (E_d), binding energies of small clusters of size $j(E_j)$, up to the so-called 'critical' nucleus of size $i(E_i)$. When large clusters can decay as well as grow, as is the case close to equilibrium adsorption conditions, then the corresponding free energies of evaporation (latent heats) in 2D (onto the substrate) and 3D (into the vapour) can also be important.

So far, figure 3 has indicated that we are concerned with two independent experimental variables (R, T_s) which together form the main way that $\Delta\mu$ can be influenced for a given system. But we also need three essentially independent types of material parameters (E_s, E_d, E_i) to describe the behaviour of the early stages of nucleation and growth, even on a perfect substrate.

Real surfaces, however, may be far from perfect, containing a distribution of ledges, kinks, dislocations and point defects, in addition to the perfect terraces. These imperfections can influence the binding of single atoms and small clusters to the substrate and via such binding changes can strongly influence adsorption, diffusion and nucleation behaviour. This is especially so if there is a high nucleation barrier (i.e. a small concentration of critical nuclei) on a perfect terrace. Then the barrier will often be by-passed on a real surface by the agency of special sites, shown schematically in figure 3 by a ledge.

Perhaps the most well-known examples are the growth on terraces at low supersaturation using dislocations, as discussed originally by Burton *et al* (1951), and the observation of the resulting spiral terraces on alkali halides by decorating the ledges with small gold islands (Bassett 1958, Bethge 1962, 1969, 1982). These two examples (cf figure 22) show the very characteristic behaviour of layer growth systems in using screw dislocations to propagate a continuous ledge and thereby avoid a nucleation barrier, and of island growth systems to use such a ledge to promote the nucleation rate by lowering the barrier dramatically.

The final set of processes illustrated schematically in figure 3 are re-arrangement processes. The clusters which initially form, at defect sites or on the perfect terrace, are not necessarily in their most stable form and can re-arrange in many different ways. Such processes can include mixing of species (alloying), shape changes caused by (surface) diffusion and/or coalescence, annealing of defects, etc. Diffusion processes thus occur at several stages of thin film formation: the motion of single atoms in forming small clusters, the mobility of these clusters themselves and the re-arrangement of larger clusters (islands) after coalescence.

Thermodynamic and Kinetic Rate Equation Based Descriptions:

After the intial successes in understanding the equilibrium thermodynamic behaviour of gases in terms of the kinetic theory of gases, one of the earliest challenges faced related to seeking an understanding of the phenomena of condensation of a vapour into liquid droplets. Gibbs, in 1878, provided[33] the first succinct thermodynamic description of the process, introducing the notion of spontaneous thermodynamic fluctuations in the local density of a supersaturated vapour giving rise to the formation of "nuclei" of the liquid phase which, if exceeding a critical size, would lead to "growth" of the liquid phase. The mechanism was termed homogenous nucleation and growth (N&G) mechanism, and a thermodynamic barrier (i.e. activation energy), determined by the relative balance of the volume and surface free energies of the condensing phase, was shown to exist for the formation of the critical nuclei. Gibbs also recognized that the growth of a crystal was different from condensation of a vapour in at least one important aspect - the periodicity of the crystal structure. He noted that since the addition of atoms to a growing crystal has to occur at a site in the crystal, the configuration of atoms in the "nuclei" presented by the crystal surface to the vapour varies periodically in time as each crystal plane is completed. Thus while the free energy of the assembly of atoms in a liquid droplet is a continuous function of the size of the droplet, it is a discontinuous function of the size of a perfect crystal.

Subsequent developments of Gibbs' notion of nucleation, employing thermodynamic descriptions, are largely due to Volmer and Weber,[34] and Becker and Doring[35]. Volmer and Weber gave a thermodynamic description of condensation of a supersaturated vapour into liquid droplets assuming that the distribution of nuclei of size $n < n_c$, where n is the number of atoms in the nucleus and n_c is the critical size, is the same as the equilibrium distribution if the vapour and liquid phase were in fact stable. To then allow for growth

initiation via the nucleation process, such a distribution of the nuclei is maintained by requiring that each nucleus reaching the size (n_c+1) be removed from the distribution of nuclei and (n_c+1) atoms be added to the vapour phase. Such a distribution, obviously of dubious physical meaning, has often been referred to as a quasi-steady state distribution. The rate at which critical nuclei are formed - called the nucleation rate - is then given by the product of the number of critical nuclei in this quasi-steady state distribution and the probability per unit time for an atom from the vapour to attach itself to one of the critical nuclei. It is self-evident that such a nucleation rate is of some value only under conditions for which little or no transformation from one phase to another has occurred. The nucleation rate, from which can be determined the growth rate of the new phase, is, however, extremely sensitive to the degree of supersaturation. It is very low until a critical supersaturation is reached, whence it increases rapidly to large values. The critical supersaturation corresponds to the breakdown of the assumption of a quasi-steady state distribution of nuclei.

Becker and Döring improved[35] on the Volmer-Weber[34] theory by explicitly recognizing that a nuclei reaching the critical size n_c has equal probability of either growing or shrinking and nuclei of size $n > (n_c+1)$ also have a finite probability of shrinking although they have a higher probability of growing on the average. They thus formulated an improved description of the problem, even though the solution obtained is not sufficiently accurate. Perhaps more pertinent to the subject of this review, while the Volmer-Weber theory applies specifically only to the condensation of a supersaturated vapour, Becker and Doring also considered growth of a solid from the vapour phase, being mindful of the previously mentioned differences noted by Gibbs. Thus they provided a theory of epitaxial growth via the nucleation mechanism assuming the shape of the crystal nuclei to be cubical. It is perhaps due to the fact that the Becker-Doring theory of growth via nucleation captures the essence of the phenomenon that nearly all

subsequent developments are derived from it, in one form or another, including descriptions of nucleation of a solid phase from a liquid or another solid phase.

A fundamental assumption of the thermodynamic description of the nucleation and growth mechanism is that the critical nuclei are sufficiently large that thermodynamic notions are applicable. For critical nuclei involving only a few atoms this is not the case and a kinetic description of the process of nucleation becomes essential. Theoretical developments along these lines are discussed later in this section. To maintain a historical perspective, we next discuss the parallel development of epitaxial growth from the vapour phase not involving nucleation as the growth mechanism.

The simplest description of growth from the vapour phase and leading to an expression for the growth rate was given in 1882 by Hertz[36] and in 1909 by Knudsen[37]. Employing the kinetic theory of gases, the rate of impingement (i.e. flux) of the vapour phase atoms on a solid surface is found to be nearly,

$$R^{+}=\{S.a_o.P/\sqrt{2\pi MkT}\} \qquad (II.1)$$

where P is the pressure at temperature T which is assumed to be the same for the vapour and the solid surface, M is the mass of the vapour specie, a_o is the area per site on the surface and S the sticking coefficient. Further, employing the thermodynamic relation,

$$\Delta\mu=(\mu-\mu_e)=k_BT\ell n(P/P_e) \qquad (II.2)$$

where μ and μ_e are the chemical potential under the chosen conditions and at equilibrium, respectively, and P_e the equilibrium pressure, one may write the attachment rate in terms of the driving force, $\Delta\mu$, as,

$$R^{-}=\{S\ a_o\ P_e/\sqrt{2\pi MK_BT}\}\ \exp\ \{(\mu-\mu_e)/k_BT\} \qquad (II.3)$$

Thus, if R^- is the net desorption rate, then the net rate of attachment is given by,

$$R = (R^{+} - R^{-}) \qquad (II.4)$$

It thus remains to find an appropriate expression for R^-. However, it is also true that at equilibrium (i.e. $\Delta\mu$=o), R=o, so that R^-=R^+($\Delta\mu$=o). Hence from equations (II.3) and (II.4) it follows that,

$$R = R^{-}\ (e^{\Delta\mu/k_BT} - 1) \qquad (II.5)$$

where

$$R^{-} = \{\ S\ a_o.P_e/\sqrt{2\pi MkT}\}$$

provided one assumes that the net evaporation rate for $\Delta\mu$=o is essentially the same as at equilibrium. We shall shortly return to a discussion of the limitations of equation (II.5).

An important feature which is not explicitly a part of the preceding considerations of crystal growth is the consequences of the atomistic nature of the solid surface and its influence on the kinetics of the atomistic processes responsible for crystal growth. In addition, the issue of when nucleation and growth is likely to be the mechanism of crystal growth initiation remains unexamined. Amongst the earliest investigators to recognize the critical importance of these issues, and the nature of the starting solid surface, in controlling the (a) kinetics, (b) mechanism and (c) the resulting surface morphology of the growth front, were Frenkel,[38] Kossel[39] and Stranski[40]. Since these are the three issues of utmost significance to this review focussing on molecular beam epitaxial growth of compound semiconductors, in the following we provide a brief background to the early developments of these notions. This should provide a helpful framework within which the reader can not only systematically examine the issues relating to MBE, but, as shall be seen, also appreciate the new elements introduced by MBE-elements which in turn demand generalization of old ideas.

To introduce explicitly the atomistic nature of solids, Kossel introduced[39], as a model, an elemental, simple cubic, solid with nearest neighbor bonds of energy ϕ - the

so called Kossel crystal. He recognized the significance of the presence of steps, kinks, ledges, etc. (see fig. 1) in influencing both the kinetics and mechanism(s) of epitaxial growth on a surface otherwise free of defects such as screw dislocations, impurities, etc. Restricting himself to considerations of the homoepitaxy of such a solid from an atomic vapour, he pointed out that growth on such surfaces will occur via addition of atoms at the kink sites on the steps since such a process is self repeating. Arrival of atoms at the kink sites is from both the vapour and through diffusion of atoms adsorbed on the flat terraces between the steps, including diffusion along step edges, the relative probability depending upon the degree of supersaturation, and substrate temperature. The fundamental atomistic kinetic processes of surface migration and desorption to the parent vapour phase, including their dependence on the local bonding configuration (i.e. number of bonds in the initial state) could, in principle, be accounted for in a kinetic equation based formulation of the growth process. However, exact analytic solutions to such equations are not possible and the results had to be obtained within a variety of simplifying assumptions. The simplest such assumption is that the evaporation rate of an atom having m nearest neighbor bonds, m = 1 through 5 representing the possible number of nearest neighbor atoms for a surface atom in the Kossel crystal, may be replaced by the evaporation rate from the kink sites (m = 3). This simplification is motivated by considerations of micro-reversibility and the view that at equilibrium (i.e. no growth), the overall evaporation rate should be well represented by the desorption rate from the kink sites since, in the preceding view, growth is *asserted* to be via attachment at the kink sites. It is thus thought fair to further assume that evaporation rate during growth is also well approximated by that from the kink sites at equilibrium. The expression for the growth rate, R, thus arrived at is:

$$R = (R^{+} - R^{-})$$

$$= (K_{eq} e^{\beta \cdot \Delta\mu} - K_{eq})$$

$$= \nu e^{-3\beta\phi} (e^{\beta \cdot \Delta\mu} - 1) \qquad \text{(II.6)}$$

where ν is the attempt frequency, $\beta = (k_B T)^{-1}$ and $\Delta\mu$ is the degree of supersaturation. Expression (II.6) thus represents the limiting value of the growth rate. Such an approximate result has been referred to in the literature as the Wilson-Frenkel growth rate, presumably because Wilson[41] in 1900 and Frenkel[42] in 1932 gave the limiting growth law for growth from the melt, even though the limiting growth law for growth from the vapour was in fact given much earlier, in 1882, by Hertz[36], and in 1909 by Knudsen[37].

Simple as the expressions (II.5) and (II.6) may be, the approximations forced to arrive at these analytic results also lead to many deficiencies. One immediately notes that for $\Delta\mu \to 0$, the growth rate is linearly proportional to $\Delta\mu$. The nucleation and growth regime is thus completely lost in the approximation. For the result (II.6), one might have anticipated this from the underlying reasoning that growth proceeds by attachment at kink sites. The atomistic reasoning, however, at least clarifies the expected regime of applicability of a result of the form (II.5). The very burden of a theory describing the nucleation and growth regime is to demonstrate how nuclei form so that, once formed, they can generate their own kink sites on the steps defining the edges of the supercritical nuclei. Approximations other than the one noted above have been tried but they all lead to some unphysical feature or another. We shall, later in this discussion, note one such approximation.

One particular assumption inherent in the preceding discussion leading to expressions (II.5) and (II.6) needs to be explicitly drawn to the reader's attention, for it has significant bearing on the subject of MBE growth to be taken up in the next section. This is the assumption that the temperature of the vapour phase species impinging upon the solid surface and that of the solid surface itself, are the same. It is only when such a condition is well satisfied that not only are the preceding considerations of some merit,

but even the central concepts of micro-reversibility and the use of relations (II.1) and (II.2) with a common temperature to arrive at (II.3), of meaning. By contrast, were one to consider growth from the vapour phase in which a nearly ballistic impingement of a vapour beam at some temperature T_v on a solid surface held at another temperature T_S were involved, then all the preceding considerations are, to say the least, called into question. The MBE growth of III-V compound semiconductors, as shall be seen in the next section, is generally carried out under growth conditions where this is likely to be the case. It is for this reason as well that considerations of MBE growth demand a fresh look at the problem with an eye not jaundiced by previous experiences and prejudices carried over from the historical literature of vapour phase crystal growth.

Burton, Cabrera and Frank furthered[43] Kossel's ideas towards an atomistic understanding of the mechanisms of epitaxial growth. These authors, noting that the measured growth rates on real crystals at supersaturations of order of, or less than, 1% were several orders of magnitude higher than predicted by theories of crystal growth on perfect substrates, concluded that "growth of crystals under low supersaturation can only be explained by recognising that the crystals which grow are not perfect and that their imperfections will provide the steps required for growth, making two-dimensional nucleation unnecessary". While the work of BCF is perhaps best remembered and widely quoted in the crystal growth literature for identifying the role of dislocations terminating in the surface with a screw component in influencing the growth rate, several other results pertaining to defect free surfaces obtained in the paper are of no less significance. In particular these authors provide a clear discussion of the relative significance of the diffusion length (l) of an adsorbed particle and the average distance between the kinks existing at the steps. The variety of considerations and results obtained by BCF are too numerous to summarise here. The interested reader is thus referred to the original paper. However, our interest here being focussed on epitaxial growth on low index, "atomically

perfect" solids, the following discussion, though not explicitly given by BCF, we believe follows as a natural, and essentially self-evident, consequence of their analysis.

The operational notion of a "perfect solid surface" is a surface for which the average separation (W_o) between the steps, inevitably present on a real surface, is much larger than the surface diffusion length (l) under the growth conditions (see fig. 2a). Thus, in a situation where $l << W_o$, growth at low supersaturation can be initiated only through surface diffusion controlled chance formation of critical clusters stable against break up caused by the atoms leaving for the parent phase - the vapour. Initiation of growth under such a condition is thus via the nucleation and growth mechanism. It is important to recognize that the critical nuclei formed may themselves be 3-dimensional or 2-dimensional depending upon the relative rates of attachment of atoms in the directions normal or parallel to the surface. Once the critical cluster size is passed, further growth can proceed via diffusion controlled migration of atoms to the step edges provided by the clusters themselves, as well as, in some cases, coalescence of mobile clusters. If the energetics of the material system and the kinetics attendant to the growth conditions are such that growth initiates via 2D nucleation, then an essentially layer-by-layer mode of material addition will result. However, with each subsequent addition of a monolayer, the average separation between the steps will decrease since statistically it is unlikely that a given layer is hundred percent complete before the initiation of the next. The net consequence is that the average terrace width $<W>$ becomes a function of time, $<W(t)>$, such that $<W(t=o)>=W_o$. Once $<W(t)>$ becomes $< l$, the surface migration length, nucleation is no longer needed for growth to continue. The arriving atoms, by and large, are able to make their way to the kinks and steps where the higher bond coordination reduces dramatically their chances of evaporation to the vapour phase or migration away from the step. Indeed, if the starting solid surface and growth conditions were such that $W_o < l$ (fig. 2b), then attachment of atoms at the kinks

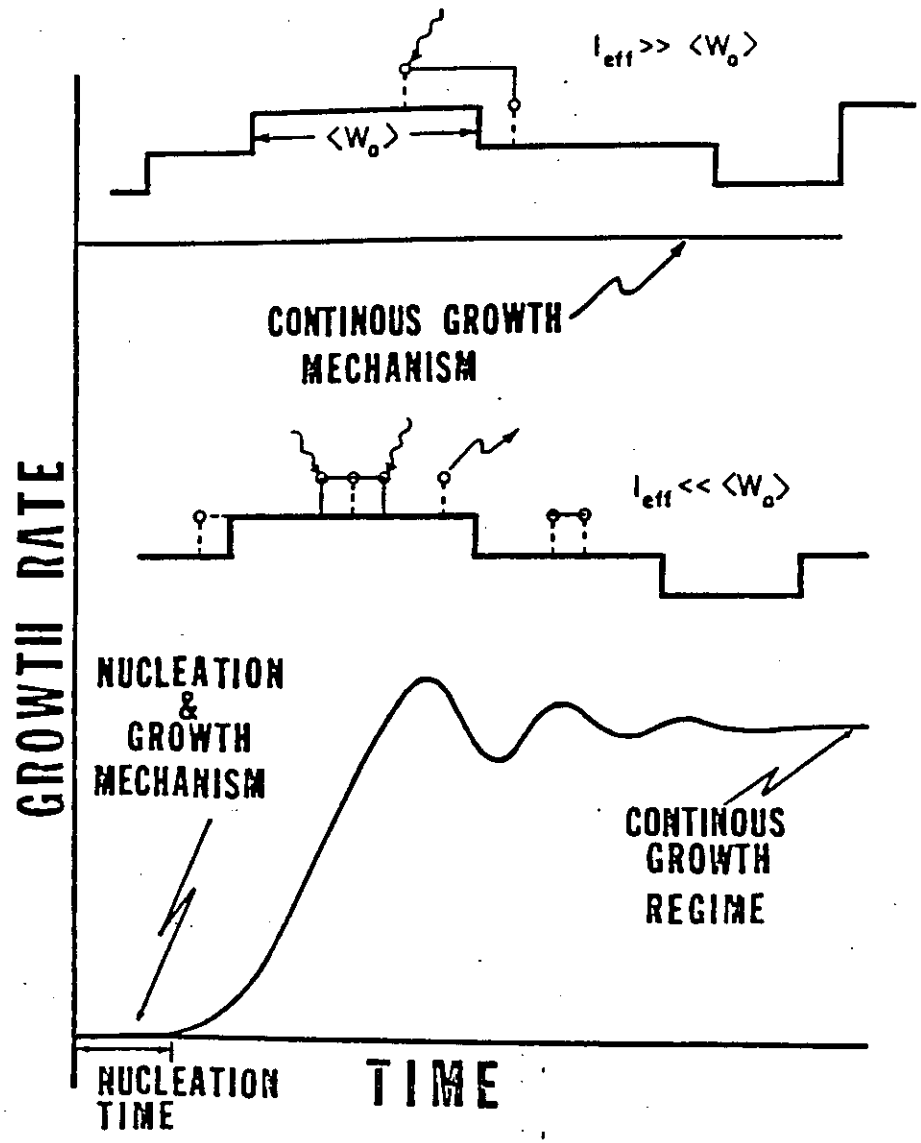

Fig. II 2

and steps is the predominant process of attachment of the atoms from the vapour to the solid phase from the very beginning and formation of critical clusters to initiate growth is no longer required. The growth mechanism in such a situation has been referred to as the continuous growth mechanism. It is then self-evident that even when nucleation may be the growth initiation mechanism, with continued growth the growth mechanism will eventually change over to the continuous growth mechanism, the time for this change over being controlled by the collective influence of individual kinetic rates on the time evolution of the surface morphology of the growth front. Figures 2(a) and (b) also show a schematic representation of the corresponding growth rate as a function of time. A feature of fundamental importance which follows from the foregoing discussion identifying the nucleation and growth and continuous growth mechanisms for growth of solids on defect free and atomically flat low index solid surfaces, and whose consequences we will have occasion to discuss later, is that for the former the surface step density distribution changes significantly with continued growth – in particular in a near oscillatory fashion – until it reaches a steady state behaviour. For the latter growth initiation mechanism, it is the step density distribution of the starting solid surface, hereafter called the substrate, which essentially gets perpetuated during growth.

Theory of nucleation and growth

In thermodynamic equilibrium all processes proceed in opposite directions at equal rates, as required by consideration of 'detailed balance'. Thus, for example, in equilibrium adsorption, surface processes such as condensation and re-evaporation, decay and binding of 2D clusters must be in detailed balance. There is thus no net growth and the system can be described by unchanging macroscopic variables, e.g. $\theta(p, T_s)$, while microscopically the system is continually changing via these various surface processes. Equilibrium statistical mechanics can be used to describe models of such situations.

By contrast, crystal growth is a non-equilibrium kinetic process and the final macroscopic state of the system depends on the route taken through the various reaction paths indicated in figure 3. The state which is obtained is not necessarily the most stable, but is kinetically determined. In general, certain parts of the overall process may be kinetically forbidden (e.g. dissolution into the substrate), others may be in 'local' thermodynamic equilibrium, and some will be kinetically rate-limiting. In the second case, equilibrium arguments may be applied locally, e.g. to the adsorption–desorption cycle so that

$$n_1 = R\tau_a. \tag{1.1}$$

Another case is the growth of small clusters which decay rapidly; this leads to the so-called Walton relation (Walton 1962) for the concentration of j clusters, where $j \leqslant i$ = 'critical' cluster size:

$$(n_j/N_a) = (n_1/N_a)^j \sum_m C_j(m) \exp[\beta E_j(m)]. \tag{1.2}$$

The $C_j(m)$ are statistical weights which can be calculated from the configurational and other contributions to the entropy of these j-sized clusters of type m; equation (1.2) can be easily derived from detailed balance or statistical mechanical considerations (Walton 1962, Venables 1973). At low temperatures only the clusters with highest binding energy E_j will be important; the Σ_m in equation (1.2) can then be truncated to one term only.

Kinetic rate equations have been used to describe nucleation and growth behaviour and interpret experiments since the first publications of Zinsmeister (1966, 1968, 1969, 1970, 1971). If only single atoms are mobile on the surface these have the form

$$dn_1/dt = R - n_1/\tau_a - 2U_1 - \sum_{j=2}^{\infty} U_j \tag{2.1}$$

$$dn_j/dt = U_{j-1} - U_j \qquad (j \geqslant 2) \tag{2.2}$$

where n_1, n_j are surface concentrations per unit area and the U_j are the net rate of capture of single atoms by j clusters.

By dividing clusters into 'subcritical', $j \leqslant i$, and 'stable', $j > i$, and summing all stable clusters via

$$n_s = \sum_{j=i+1}^{\infty} n_j$$

these equations can be simplified (Venables 1973) to

$$dn_1/dt = R - n_1/\tau_a - d(n_s w_s)/dt \tag{2.3}$$

$$dn_j/dt = 0 \qquad (2 \leqslant j \leqslant i) \tag{2.4}$$

$$dn_s/dt = U_i - U_c - U_m. \tag{2.5}$$

In equation (2.3) the last term represents the loss of single atoms to n_s stable clusters with an average number of atoms w_s per cluster. Equation (2.4) is a consequence of the detailed balance arguments ($U_j = 0$) for the subcritical clusters which leads to the Walton relation (equation (1.2)). The last two terms in equation (2.5) are attempts to deal with coalescence; if stable clusters impinge on each other by growth (U_c) or

The number of stable clusters has often been equated with the number of islands observed by transmission electron microscopy (TEM). Using this technique, the number, average size and shape, plus size and spatial distributions can be measured in great detail.

The critical cluster size i is the size which is most unstable: clusters of size $> i$ tend to grow rather than decay, whereas for $j < i$ decay is more probable and local equilibrium tends to hold. one finds, for example, in the island growth mode, that $\Delta\mu (= kT_s \ln(p/p_e)$, where p_e is the equilibrium vapour pressure of the bulk deposit) is often extremely high and consequently i is very small, often only a few atoms.

The instantaneous condensation coefficient $\beta(t)$† is simply given from equation (2.1) by

$$\beta(t) = 1 - n_1(t)/R\tau_a. \tag{2.12}$$

The integrated condensation coefficient $\alpha(t)$ is

$$R t\alpha(t) = R\int_0^t \beta(t')\,dt'$$

$$= Rt - \tau_a^{-1}\int_0^t n_1(t')\,dt'. \tag{2.13}$$

In the case of island growth where R can often be reduced to zero without the stable clusters disappearing, $Rt\alpha(t)$ can be equated experimentally with the total number of atoms in stable clusters, i.e. $(n_s w_s)$. This follows from equation (2.3) and the definition of $\alpha(t)$. In the case of layer growth and particularly of equilibrium adsorption, care should be exercised, since the amount remaining condensed may well depend on R; the deposit may disappear if the incident flux is turned off.

The experimental observables n_s, Z, α and β can be measured as a function of t, T_s and R by a combination of (electron) microscopic and surface physics techniques. If single atoms only are mobile and nucleation takes place at random positions on the perfect substrate, the nucleation and growth behaviour should be interpretable in terms of the rate equations described in this section. Time, temperature and deposition rate dependencies should be mutually consistent and parameters deduced from such experiments, for example E_a or E_d, should agree with independent measurements where they exist.

The various regimes predicted by the rate equations can be discussed physically with the help of figure 5, chosen for high (a) and low temperatures (b). Initially $n_1 = Rt$, α and β are equal to 1 and n_s and $Z = 0$. This is the 'transient' regime. For high temperatures, with τ_a small, this lasts for $t < \tau_a$ and the value of n_s at $t = \tau_a$ is negligible. For low temperature, n_1 is limited by capture at stable clusters at $t = \tau_c = (\sigma_s D n_s)^{-1}$ and n_s can be sizeable.

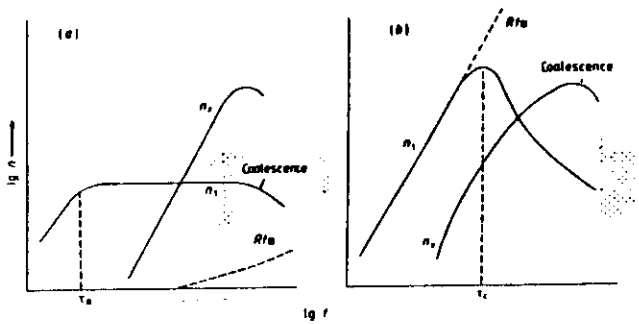

Figure 5. Evolution of the single-atom density (n_1), the stable cluster density (n_s) and the total number of atoms condensed ($Rt\alpha$) as a function of deposition time t for (a) high temperatures and (b) low temperatures. The re-evaporation time τ_a, capture time τ_c and limitation of n_s by coalescence are indicated.

A third example is using thermodynamics to describe the shape of the islands formed in terms of surface and interfacial free energies. The equilibrium form of crystals of A condensed on B can be described in terms of the surface free energies, γ_A, γ_B and the interfacial free energy γ^* between A and B. The equilibrium form can then be calculated via the Wulff theorem;

To illustrate the change of crystal orientation, a simple example is given in Fig. 1: a crystal of cubic equilibrium shape is put on a substrate, of which γ_B^* is assumed to be isotropic. Configurations of minimum volume are shown for various values of γ_B^*; the parameter s is γ_B^* scaled by γ_A of {100} face:

$$s = \frac{\gamma - \gamma_B}{\gamma_A(100)}$$

For $s<-1$ the crystal wets the substrate completely. For $-1<s<-0.85$ a thin square plate appears, as usually assumed to be the case. As s increases, the crystal tends to reduce the exposed volume by changing its orientation; the following axes become perpendicular to the substrate: ⟨111⟩ for $-0.85<s<-0.32$, ⟨110⟩ for $-0.32<s<0$, ⟨100⟩ for $0<s<0.83$, ⟨110⟩ for $0.83<s<1.01$, ⟨111⟩ for $1.01<s<1.73$. Note that the crystal is not detached from the substrate, even if $s>1$. The crystal orientation, thus determined, is a preferential orientation without a structural fit. For $s>1.73(\sqrt{3})$ the crystal becomes detached from the substrate.

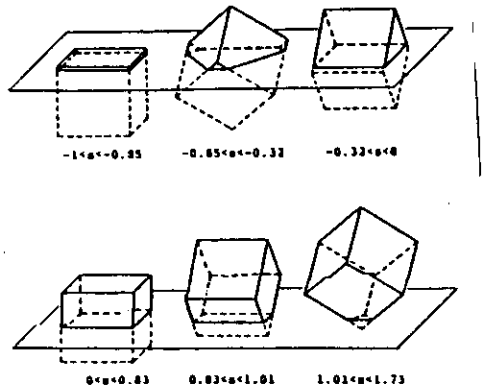

CHAPTER II

ATOMIC SCALE SIMULATIONS

I. INTRODUCTION

In this lecture we give a survey of the role of Monte Carlo (MC) simulations in the science of crystal growth. Characteristic for MC simulation is its stochastic nature: random numbers will determine whether and how a system changes its state. This should be done according to transition probabilities which are determined from a model of the physical system of interest. Fluctuations are automatically included, in contrast to most other theories which are deterministic and give, therefore, only the average time development.

Firstly we assume that the changes in the system (e.g. particles attaching to the crystal) take place so fast that intermediate states can be neglected. Therefore we restrict ourselves to discrete simulation, i.e. simulation of a system with a discrete set of states.

Secondly we intend to describe crystals, growing from some surrounding phase which may be fluid or gaseous. This allows us to define a lattice with the crystal symmetry, whose cells are either solid or belong to the ambient phase. We shall not go into detail concerning the ambient phase. We assume that it is homogeneous and that the concept of the chemical potential of a particle which is going to join the crystal can be used.

The aim of simulation is to describe the time development of a system when the probabilities of some "elementary events" are known. In our case three types of elementary events come into consideration: addition (also called attachment, condensation or creation), subtraction (detachment, evaporation, dissolution or annihilation) and migration (diffusion) of single solid cells.

Discrete Monte Carlo simulation has a number of different aspects and can therefore be used for several purposes:

(i) It can be seen as an ideal experiment with a simple, perfectly known system. Several effects can be studied independently, e.g. nucleation, growth spirals, surface diffusion, temperature, crystal structure etc.
(ii) It solves the master equation of the system (which governs its time evolution), numerically. Usually both high and low temperature approximations fail close to transition temperatures, such that MC simulations may be the only possibility which is left.
(iii) In addition to (ii) it can be used to show that the results of analytical theories are often applicable, even when their presuppositions are already valid. Their domain of validity is, in such a way, checked and even extended.
(iv) Simulation of a concrete physical experiment may give a better insight to the relevant atomic processes and may stimulate further experimental investigations and the development of new ideas and models.
(v) Observation of a fluctuating system may reveal unexpected effects which may have general implications. The no man's land between theory and experiment can be reduced.

Monte Carlo simulations in the field of crystal growth have been proved very useful in the study of equilibrium surface properties and growth mechanisms like normal growth, nucleation growth, spiral growth etc. The first simulations were carried out by Chernov (5,6) and Binsbergen (7,8) between 1966 and 1971. After 1971 the number of people involved with simulations increased rapidly

THE RATE EQUATIONS

In simulating the phenomena of vapor deposition on an initially specified crystalline surface, the following fundamental atomic processes are assumed:

(a) *Condensation* of a vapor atom on a "crystalline" site or "deposited-layer" site (vapor atom→adatom);
(b) *Evaporation* of an adatom to the vapor (adatom→vapor atom);
(c) *Migration* of the adatom to a neighboring site (adatom→adatom).

The pertinent rate equations for these processes will now be presented.

The rate at which condensation occurs is directly proportional to the rate at which atoms strike the surface. The number α of vapor atoms striking a unit area of a surface per unit time is given by

$$\alpha = P/(2\pi mkT)^{1/2} \tag{1}$$

where P is the vapor pressure, m is the mass of the vapor atom, and k is the Boltzmann constant. From the expression for the chemical potential μ of an ideal gas,[9]

$$\mu = -kT \ln[(2\pi mkT/h^2)^{3/2}(V/N) f_v(T)]$$

we obtain

$$\alpha = kT[(2\pi mkT)/h^2] \exp(\mu/kT) f_v(T), \tag{2}$$

where $f_v(T)$ is the internal partition function for atoms in the gas phase. Fowler[9] derived an equation using statistical mechanics for an ideal lattice gas system on a two-dimensional uniform lattice with no interaction between nearest-neighbor adsorbed atoms. Fowler's treatment gives rise to an interesting expression for the rate of evaporation of gas atoms from the lattice surface:

$$\nu = k_0 \exp(-E/kT), \tag{3}$$

where

$$k_0 = [(2\pi mkT)kT/h^2][f_s(T)/f_v(T)]$$

E is the binding energy per particle per site; $f_s(T)$ is the internal partition function for particles in the adsorbed phase which is assumed to be independent of the local environment of the adsorbed particle. (This is not necessarily realistic since f_s depends on the number of degrees of freedom of a particle, which varies with the number of nearest neighbors.)

Equations (2) and (3) are quite similar. In fact, using these equations to form the ratio of the rate at which particles strike the surface to the rate at which they evaporate yields

$$\alpha/\nu = \exp[(E+\mu)/kT]. \tag{4}$$

Note that we have set $f_s(T) = 1$ in deriving Eq. (4).

In computer simulation of the nonequilibrium behavior of a system, the relative rates for the various processes must be known. Equation (4) expresses the needed relative rate for adsorption and evaporation. We further assume that the nearest-neighbor interactions and next-nearest-neighbor interactions affect only the energy of the interaction E and not the form of Eq. (4). That is to say,

$$E = -\epsilon - \eta w - \eta' w' \tag{5}$$

where ϵ is the binding energy of a site, η, η' are the number of nearest-neighbor and next-nearest-neighbor atoms, respectively, and w, w' are the nearest-neighbor and next-nearest-neighbor lateral interaction energies.

For the square lattice, lateral interactions between next-nearest neighbors are said to exist when sites located on opposite corners of a square are occupied. The interaction forces are assumed to be van der Waals–London, with the primary attractive interaction energy falling off as the sixth power of the distance between adsorbate atoms. For the square lattice, where the ratio between distances separating next-nearest and nearest neighbors is $r_2/r_1 = \sqrt{2}$, it follows that $w_2/w_1 = \frac{1}{64}$ where w represents the interaction energy.

IV. THE COMPUTER SIMULATION MODEL

In the Vapor Deposition Simulation (VDS) programs, the surfaces on which vapor atoms are adsorbed are two-dimensional square lattices.

Periodic boundary conditions are used; i.e., for a $N \times N$ lattice, $X_1 = X_{N+1}$ and $Y_1 = Y_{N+1}$.

We assume that the binding energy of an adsorbed atom to the substrate is related only to the number and type of atoms it "touches." We assume that there exist only two types of atoms: the crystalline surface atoms and the vapor atoms. The atoms are the same size so that the deposited atoms will retain the crystal packing.

The crystalline surface atoms are fixed once their positions are specified at the beginning of the problem. We will denote these atoms by "B." The depositing atoms may condense, evaporate, or migrate. We will denote these atoms by "W." E_{WB} denotes the binding energy for "B" and "W" atoms which are touching. E_{WW} denotes the binding energy for two touching "W" atoms. The total binding energy equals the sum of the binding energies of the single bonds.

Evaporation

The evaporation of an atom requires that the bonds between it and its neighbors be broken. The evaporation rate per atom ν_e is a function of the binding energy, E; $\nu_e = \exp(E/kT)$. Examples of the binding energy for some evaporation configurations are presented in Fig. 1(a)–(c).

Migration

The migration of an atom requires that some bonds, but not all of the bonds, be broken in order to go to another site. This depends on the particular geometry for the migration. A particular example is given in Fig. 1(d).

The migration of the W adatom to (a) positions 1, 2, 3, or 4 requires $2B$–W bonds to be broken, i.e., $\epsilon_m = 2E_{WB}$ (no nearest-neighbor adatoms);

The following "normalized" rate expressions are used.

$$\nu_a/\alpha = \exp[(\epsilon+\eta\omega-\mu)/kT] \quad (8)$$

$$\nu_m/\alpha = \exp[(\epsilon_m-\mu)/kT] \quad \text{(migration)}, \quad (9)$$

where ϵ_m is the energy associated with the bonds broken in order for the adatom to migrate to the neighboring site.

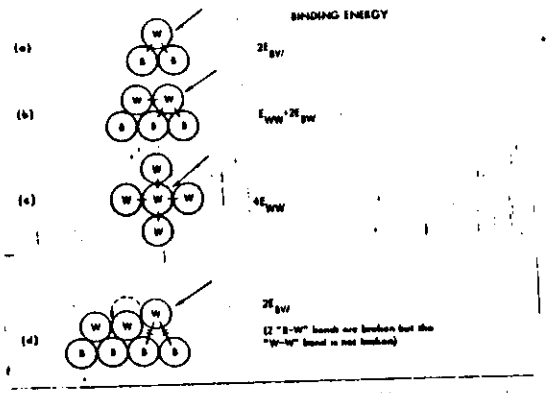

FIG. 1. The binding energy for different geometrical configurations and transitions. Figure 1(c) depicts the sites to which the W adatom may migrate for monolayer transitions.

V. THE METHOD OF SIMULATION

As indicated earlier, the use of random numbers is employed to control the various movements of a dynamical system of atoms evaporating, condensing, and/or migrating on the surface of a lattice. The VDS programs are thus based on Monte Carlo methods. Monte Carlo methods are methods of using random numbers to solve problems in applied mathematics. Their importance rests largely on the availability of high-speed electronic computers.

The crystal growth is simulated on a $20a \times 20a$ section of the surface. Periodic boundary conditions are used to help eliminate edge effects, and these conditions can be altered to force a fixed number of steps into the section. The surface configuration is retained in the computer memory by specifying its height above each of the 400 lattice points of the section. It is represented by a singly subscripted array of integers $S(I)$ with $1 \leq I \leq 440$. The 400 integers $S(I)$, $21 \leq I \leq 420$ give the surface height in interplanar spacings, and the remaining 40 integers are used for maintaining the boundary conditions. The lattice position associated with a given subscript I is indicated in Fig. 13. The four nearest neighbors of a given position labeled with I are in the positions corresponding to $I+1$, $I-1$, $I+20$, and $I-20$. A (100) surface results if we keep the top row $[S(I),\ 1 \leq I \leq 20]$ identical to the next to the bottom row $[S(I),\ 401 \leq I \leq 420]$ and the bottom row identical to the next to the top row. Whenever a surface height in the next to the top row is changed, for example, the corresponding position in the bottom row is changed to the same value, thus maintaining the two rows identical during the simulation.

The time evolution of the system is described by a series of events defined exactly as in Abraham and White's program. A random number IX is generated and normalized to give an integer I in the interval $21 \leq I \leq 420$; this determines the surface position at which a transition will be attempted (an advantage of a single subscript I is that only one random number and one normalization process is required to pick a site on the surface). A second random IY is generated to determine what transition, if any, will occur at the selected site. To save computer time, IY is left unnormalized; the generator used in this program produced numbers distributed uniformly over the interval $0 \leq IY \leq IY_{max}$, where $IY_{max} \approx 2\times10^9$. This interval is divided into three major subintervals, with the length of each proportional to the maximum possible value of the transition probability per second for the corresponding process (see Fig. 14). Then

$$L_A = \frac{(k_i)_{max}}{(k_i)_{max}+(k_{ij})_{max}+(k_i^*)_{max}}\, IY_{max}$$

gives the magnitude of the interval corresponding to an annihilation attempt, for example. In the simulations of this paper, the maximum rate constants are associated with isolated adsorbed molecules, i.e.,

$$(k_i)_{max} = k_0, \quad (k_{ij})_{max} = k_{00}, \quad (k_i^*)_{max} = k_0^* .$$

The interval in which IY falls determines which process will be attempted. To decide whether to actually execute the process, each of these intervals is further divided into two subintervals with the length of one proportional to the transition probability per second for the particular type of site which exists at the selected position; for example,

$$L_{A,i} = \frac{k_i}{(k_i)_{max}+(k_{ij})_{max}+(k_i^*)_{max}}\, IY_{max} = \frac{k_i}{(k_i)_{max}}\, L_A$$

is the subinterval corresponding to annihilation of an S_i site. If IY falls within this interval, the growth unit is annihilated; if not, the growth unit remains. In either case the event is complete and a new pair of random numbers is chosen for the next event. A slight complication occurs when IY falls in the surface diffusion interval, since a neighboring position must also be chosen in order to determine k_{ij} and $L_{D,ij}$. A third random number IZ is generated and the region $0 \leq IZ \leq IZ_{max}$ is divided into four equal intervals corresponding to the four nearest neighbors. A nearest-neighboring position is thus chosen for the diffusion jump. As before, if IY falls outside the subinterval $L_{D,ij}$, the diffusion jump is not executed and the computer proceeds to a new event.

ROUGHNESS

A characteristic property of surfaces which is intensively studied, is their roughness r^0, defined as the interface contribution to the total number of solid-fluid neighbours, per surface particle. For a solid on solid model this is the total number of such pairs, for unrestricted models one has to correct for solvent inclusions and solid islands in the bulk phases.

It can be noted that interactions and temperatures do not occur separately in the simulation, but only as ratios. There is, however, in the literature no consistency in the use of such ratios to characterize the range of temperatures and interactions which is considered. We shall choose such a ratio (denoted by θ) with the following properties: (i) for a given system θ is proportional to T; (ii) different systems at the same temperature and with the same average potential energy between two cells have the same θ; (iii) θ is scaled in such a way that the critical temperature of a two dimensional square Ising system with nearest neighbour interactions $\theta_c \approx 1$.

Point (ii) is inspired by the assumption that a system with complicate interactions can, to some extent, be approximated by a system with nearest neighbour interactions only, which are such that the total lattice energy is the same. We refer to θ as standard temperature.

Let L be the difference in enthalpy per solid cell, to be obtained from eq. (10), between one state in which all solid cells are so far away from each other that they have no mutual interaction any more, and another state where these cells are combined in a completely solid crystal. Then we define θ by

$$\theta = 0.88138\, zkT/L \quad (26)$$

where z is the number of nearest neighbours in the lattice. For convenience of the reader we give in Table 2 the relation of θ with the interaction parameters ω, ζ, α, γ and L/kT which are used by other authors.

Table 2. Relation of θ with interaction parameters of other authors

parameter	$\omega = \phi/kT$	$\zeta = J = \phi$	$\alpha = \gamma = \zeta L/kT$	L/kT
Ref.	5,6,11-14,21, 23,28,31	4,7-10,16-18,24,26,27 29,30,32,34	1,15,19,20 22	2,3,25,33
Kossel (100)	0.88/θ	1.76/θ	3.53/θ	5.29/θ
f.c.c. (100)	0.88/θ	1.76/θ	3.53/θ	10.58/θ
f.c.c. (111)	0.88/θ	1.76/θ	5.29/θ	10.58/θ
b.c.c. (100)	0.88/θ	1.76/θ	3.53/θ	7.05/θ

In Fig. 4 the variation of r^0 with temperature is shown for different crystal structures. The Kossel (100) (11) and f.c.c. (100) (24) faces have the same lateral structure, a square lattice with isotropic nearest neighbour interactions. Therefore their r^0 are similar at low temperatures. At higher temperatures, however, the difference becomes more important, mainly because the SOS condition for the f.c.c. (100) is a much stronger restriction than for the Kossel (100) face).

Also the unrestricted sc (100) face (17) is equivalent with the Kossel (100) face at low temperatures. Upon increasing the temperature, however, the solid and fluid phases become less and less distinguishable until, at the critical temperature θ_c^D = 2.00 of the three dimensional Ising model, the interface vanishes and $r^0 \to 0$.

The orthorhombic crystal (21) has, at the same temperature θ, stronger bonds in one lateral direction (weaker ones in the other) than in the Kossel crystal (here ϕ_x/ϕ_y = 3), which leads to many of neighbours parallel to the weak interactions.

The f.c.c. (111) face (25), finally, has a triangular structure, such that cells are more strongly bound in the lateral direction, which is also reflected in the higher critical temperature θ_c^{2D} = 2.07 of the two dimensional triangular Ising model and a much smaller roughness.

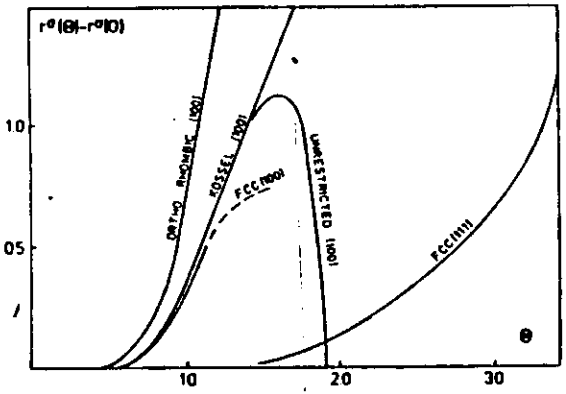

Fig. 4. Interface roughness as function of temperature for different crystal structures: orthorhombic (21), Kossel (11), unrestricted (17), f.c.c. (100) (24) and f.c.c. (111) (25).

The dynamics of crystal growth from the vapor are simulated by two basic events; impingement and evaporation. In terms of the chemical potential μ, the deposition rate is

$$k^+ = \nu \exp(\mu/kT), \tag{1}$$

where ν is the frequency factor, T is the absolute temperature, and k is Boltzmann's constant. This is obtained using the dilute-solution approximation relating the chemical potential and the concentration C in the vapor

$$\mu - \mu^{(e)} = kT \ln C/C^{(e)}, \tag{2}$$

where the superscript denotes an equilibrium quantity. The impingement rate is independent of the local surface structure.

Evaporation, or the removal of an atom from the surface, proceeds with a frequency

$$k^- = \nu \exp(-n\phi/kT), \tag{3}$$

where n is the number of bonds to other atoms of the crystal and ϕ is the energy required to break one bond. Here evaporation is treated as a simple activated process. Equilibrium prevails when the average rate of impingement is balanced by evaporation, so that the number of atoms in the crystal remains essentially constant over long periods of time. The chemical potential required for equilibrium is $\mu^{(e)} = -Z\phi/2$, where Z is the number of nearest neighbors of an atom in the bulk.[4] The corresponding impingement rate is equal to the rate of evaporation from a surface site with exactly half of the neighbors present, the kink site. Most crystals are grown under conditions where the impingement and evaporation fluxes are approximately equal, although molecular beam growth often occurs with very little evaporation flux.

This model has provided much information about the nature of the surface roughening transition for crystal faces in equilibrium with the vapor.[5] At low temperatures the important states are those in which the surface is essentially flat with only a few adatoms and vacancies. Configurations are improbable that involve large differences in the heights of neighboring sections of the surface. At higher temperatures height deviations become more likely, and whole regions may be displaced from their position at $T = 0$. This is illustrated in Fig. 1 with some typical surfaces generated by the Monte Carlo simulations with $\mu = \mu^{(e)}$ [illegible] and shows a definite change in the connectivity of the clusters between $kT/\phi = 0.59$ and 0.66. At the lower temperature only distinct adatom and vacancy clusters are present, but at the higher temperatures connected clusters extend over the entire surface. As a result, the ground state reference level of the surface is lost.

Surface roughening clearly eliminates the possibility of producing "perfect" monolayer superlattices. However, multilevel surfaces are also produced by crystal growth processes, even at temperatures far below T_c. Figure 2 illustrates a series of configurations generated at a temperature $T = 0.25\phi/k$ and $\mu - \mu^{(e)} = 2kT$.[6] The surface with $\mu = \mu^{(e)}$ is almost perfectly flat at this temperature; the only deviations are those caused by a few adatoms, vacancies, and very small clusters. Figure 2(A) is a configuration just after an equilibrium surface was placed in contact with the supersaturated vapor. A few clusters are present and the larger ones are near the critical size for 2D nucleation. At a later time, [Fig. 2(B)] clusters that nucleated earlier have expanded to a large, stable size and others have nucleated. In the final configuration shown [Fig. 2(D)] clusters are present on top of the earlier ones and material is being deposited on two levels at the same time. After reaching the steady-state structure, a number of different levels are exposed to the vapor, and a perfect layer-by-layer control of the composition is again not possible.

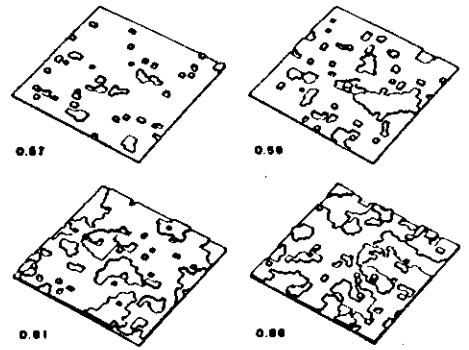

Fig. 1. Typical configurations of the simple cubic (100) face generated by the Monte Carlo simulations in the case of a crystal in equilibrium with its vapor. Small clusters and atoms with fewer than three bonds and equivalent vacancy configurations are not represented. The numbers adjacent to the figures are the values of kT/ϕ.

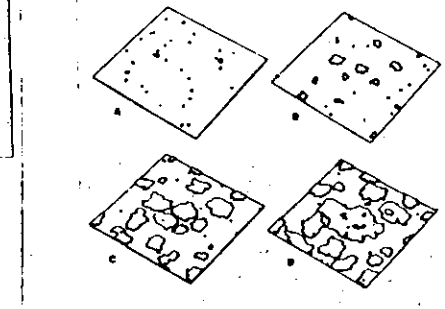

Fig. 2. Configurations of the simple cubic (100) face following the application of the driving force $\mu - \mu^{(e)} = 2kT$. Here $kT/\phi = 0.25$.

La rugosité de la surface est caractérisée par la hauteur quadratique moyenne des défauts:

$$h = ((z - z_m)^2)^{1/2},$$

où z_m est l'altitude du plan moyen.

La simulation de l'évolution de la hauteur quadratique moyenne des rugosités $h_K(\theta)$ est faite pour plusieurs valeurs du paramètre K

$K = \nu_1/n_\infty S$ qui ne dépend que de la mobilité des adatomes sur la surface, lorsque la vitesse de condensation est constante (n_∞).

Pour un adatome isolé sur une terrasse (001), on suppose que la fréquence de saut ν_1 est déterminée par la température T et une énergie d'activation E selon une loi d'Arrhénius:

$$\nu_1 = \nu_0 \exp(-E/kT).$$

Les courbes $h_K(\theta)$ obtenues sont représentées sur la figure 1. On constate qu'elles possèdent une partie initiale commune dans laquelle h croit rapidement lorsque θ augmente. Cependant, dans ce même domaine le nombre de liaisons coupées $N_K(\theta)$ diminue lorsque K augmente, pour une valeur de θ donnée. Ce résultat correspond au fait que les premiers atomes condensés sont toujours adsorbés dans la première couche atomique sur la surface — d'où la valeur de $h(\theta)$ indépendante de K — alors que l'accroissement de mobilité des adatomes permet la formation de germes bidimensionnels de plus en plus gros, entrainant la diminution du nombre de liaisons coupées lorsque la température augmente pour un même nombre d'atomes condensés sur S.

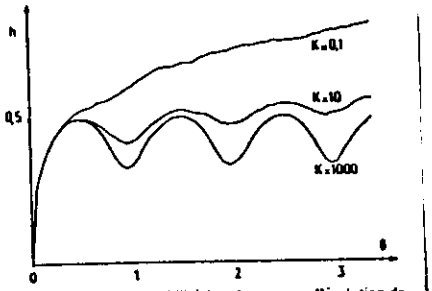

Fig. 1. Influence de la mobilité des adatomes sur l'évolution de l'amplitude quadratique moyenne des rugosités pendant la croissance simulée des premiers plans atomiques sur une face dense.

5. NORMAL GROWTH

Other current names for this growth mechanism are continuous growth and liquid-like growth. It takes place on relatively rough surfaces and a characteristic feature is that the growth rate R depends linearly on the supersaturation for small supersaturation. We define R as the number of layers added to the crystal per unit time and we normalize it usually by dividing R by the frequency k^+ of attachment.

It can readily be shown (4) that, if the surface of a mono-component crystal retains its equilibrium structure then

$$R/k^+ = 1 - \exp(-\beta\Delta\mu) \qquad (30)$$

This equation is known as the maximal or Wilson Frenkel law. The linear behaviour for small $\beta\Delta\mu$ is immediately found from a Taylor expansion of the exponential function. In Figs. 7 and 8 it is seen that we have linear growth curves for $\theta < \theta_R \approx 1.0$, but they are below the maximal law eq. (30).

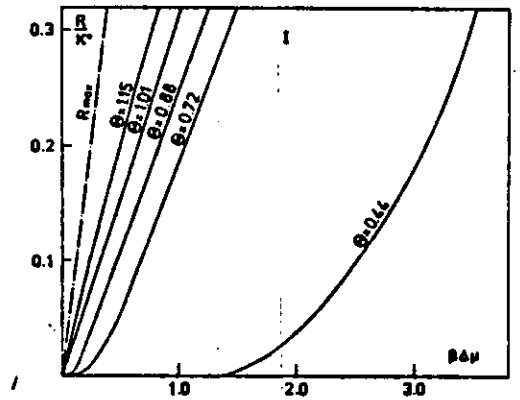

Fig. 7. Growth rate of a Kossel (100) face at different temperatures (4,33) for $\theta < \theta_R$ a "nucleation dip" at low supersaturation $\beta\Delta\mu$ is seen. The symbol I denotes the standard deviation.

It is clear that the surface cannot retain its equilibrium structure during all stages of growth, unless it is very rough. In Fig. 4 it can be seen that at θ_R the roughness is ≈0.3 which is considerably below e.g. the maximal roughness 2.0 per layer, so the surface structure will still play an important role.

The right hand side of eq. (30) is exactly the rate of growth of a kink site (German: halb Kristallage), i.e. a site at which addition or subtraction of a solid cell does not change the broken bond energy ε_{bb} (for a Kossel crystal this means that the number of solid-fluid neighbours remains constant). Figures 6 suggest that eq. (30) should be modified into

$$R/k^+ = A(\theta, X_s)(1 - \exp(-\beta\Delta\mu)) \qquad (31)$$

and we propose the following interpretation of the proportionality constant A:

$$A(\theta, X_s) = A_0(\theta)\,\frac{1 + X_s^2}{1 + X_s^2 A_0(\theta)} \qquad (32)$$

The first factor describes the growth rate when surface diffusion is absent and we see that it increases from 0.4 at the roughening temperature $\theta = 1$, to 1.0 if $\theta \to \infty$. We suppose that it is proportional to the contribution of sites which are suitable for growth. Let us call these generalizations of kink sites, active sites, then A_0 should be the concentration of active sites on the surface (which is considerably larger than the concentration of kink sites (4)).

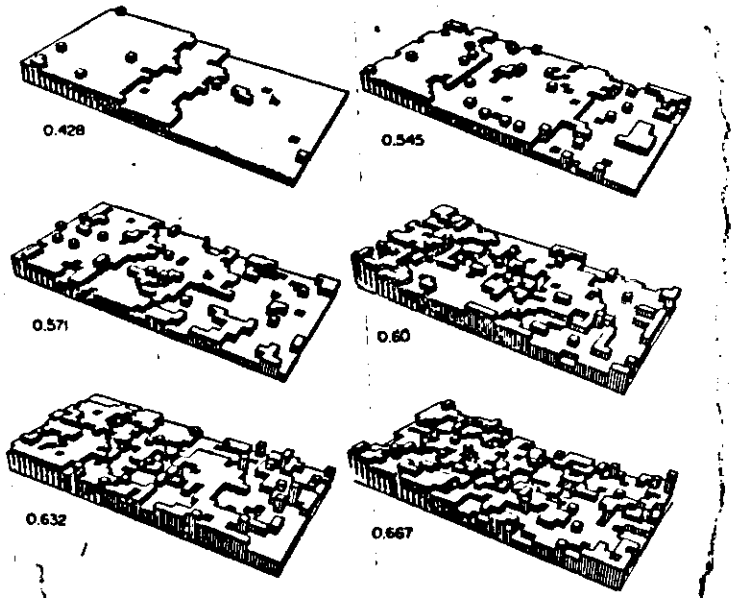

Fig. 6. Interface structure at different temperatures (43), showing the "disappearing" of a (10) step at temperatures above θ_R on a Kossel (100) face. Temperature θ (left to right, top to bottom): 0.75, 0.96, 1.01, 1.06, 1.11 and 1.18.

The roughness of a face is of major importance for the growth mechanism. Roughly speaking, normal growth takes place on rough surfaces, on smooth surfaces steps have to be generated (high index faces, nucleation, growth spiral). Therefore the roughening transition from "smooth" to "rough" faces has received much interest

NUCLEATION AND GROWTH

Figure 3 shows a comparison of the initial growth rates as a function of the time after the supersaturation is applied, as calculated by the Monte Carlo model. Figure 3(A) corresponds to the pure system. The initial rates are quite small in the case of the pure system, since the equilibrium surface structure includes few clusters where impinging atoms can stick to the crystal

As the clusters expand, however, the deposition rate increases and reaches a maximum at the point where many large and distinct clusters are present. As the clusters merge to complete the first layer, the rate diminishes, and a damped oscillatory behavior is observed. The amplitude of the oscillations is a direct indicator of the degree to which the surface is localized at one level. As more layers are deposited, statistical variations in the nucleation rate cause different regions of the surface to reach different levels, and the oscillations disappear.

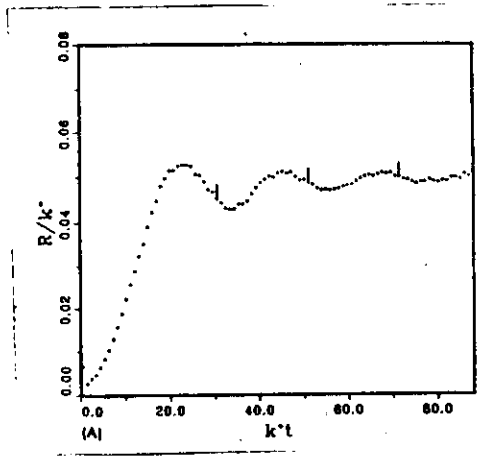

FIG. 3. (A) Growth rate transients corresponding to the growth of a perfect crystal without impurities

The time development of the number of particles in the largest cluster present on the surface, and of the total number of particles (coverage) is shown in fig. 1. The three stages of the nucleation process are readily visible. First the coverage increases from an initial value to the value in the metastable state, corresponding to the imposed supersaturation. This period corresponds to the transient time τ_t, after which on a large surface steady state nucleation would take place. Then, during the metastable period, the number of particles in the largest cluster grows steadily till finally, at time τ_+, this cluster becomes supercritical and starts growing rapidly. An unexpected feature of these curves is the linear time dependence of the area of a supercritical cluster, which contradicts the usual assumption that growth is proportional to the perimeter of the cluster.

Increasing the supersaturation, the nucleation time decreases until at a transition value β^* the growth gets a continuous character (normal growth). An example is shown in fig. 2. The largest cluster curve remains far below the coverage curve, indicating that many clusters are formed at the same time. Finally, all these clusters coalesce and the layer is filled.

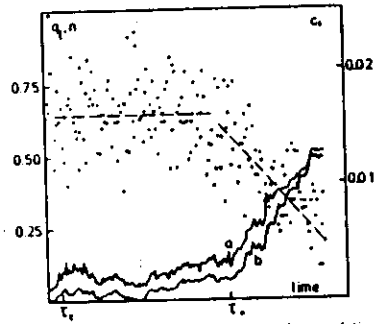

Fig. 1. Time development of the relative size n of the largest cluster relative to the total surface (b) and the coverage q_i (a). After a transient time τ_t a constant coverage remains till τ_+. In this period the adsmit concentration c_1 is about constant (dots, dashed line). This graph is typical for nucleation growth in our experiments: $\omega = 1.0\ \beta = 0.12$, 40 × 10 matrix.

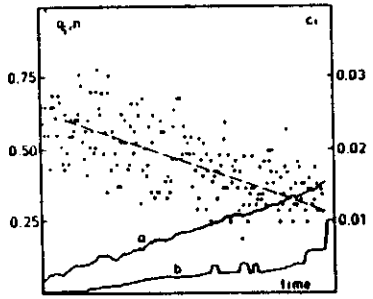

Fig. 2. Time development of the relative size n of the largest cluster (curve b) and the coverage q_i (curve a) under continuous growth conditions: $\omega = 1.0$, $\beta = 0.5$, 40 × 40 matrix.

Therefore, we propose the following alternative. The advance velocity of any curved edge is controlled by two different mechanisms: (i) the edge tends to form facets and (ii) the growth takes place mainly in concave parts of the step (growth regions). The first assumption is supported by the behaviour of a step which was originally straight, along the (11) direction. The tendency to form facets is clearly visible in fig. 9.

If the tendency to form facets is also present on the edge of supercritical clusters it is clear that usually only a few concave parts can be present, due to the small dimensions of the clusters. In view of assumption (ii) we can associate now the growth levels with the presence of one, two or three growth regions on the edge of the cluster.

Also a third observation which cannot be understood by the classical treatment is now easily explained. In fig. 10 we show the growth of two supercritical clusters where discontinuities in the spreading velocity are seen. One cluster first grows rapidly, then very slowly (disappearance of a growth region) and after some time it starts growing again (appearance of a new growth region). The other cluster first grows by a certain spreading velocity and at a certain time this velocity increases abruptly with a factor 2 (addition of a new growth region).

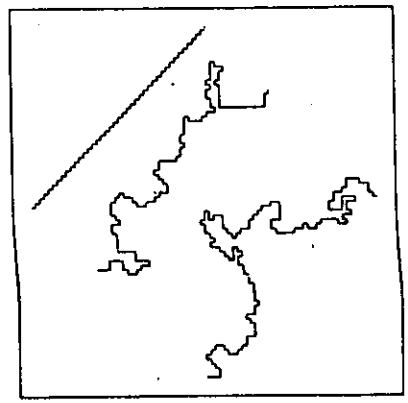

Fig. 9. The time development of an initially "straight" (11) step, which is constrained by the boundary conditions on a 40 × 60 matrix: $\omega = 1$, $\beta = 0.1$. Step patterns after 100 and 200 creations per site show the tendency to facet during growth.

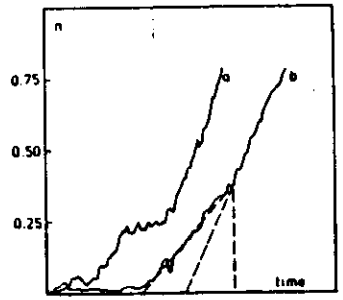

Fig. 10. Time evolution of the size (n) of the largest cluster. It can be seen that spreading may stop for a while (curve a: disappearance of the growth region) or that the spreading rate increases by a factor 2 (curve b: appearance of a second growth region). (a) $\omega = 1$, $\beta = 0.125$, 40 × 40 matrix; (b) $\omega = 1$, $\beta = 0.1$, 40 × 40 matrix.

The crystal-surface is represented in a rectangular coordinate frame with the x–y plane coinciding with the flat initial surface, or substrate. The (x, y) coordinates of the nucleation events are generated as pairs of random numbers in the interval between 0 and l. The time between events is calculated with a third such random number Z_t, using the relation

$$\Delta t = -\ln(Z_t)/Jl^2 .$$

Clusters nucleate at random sites on the surface of the crystal and at a rate J per unit area. J is a fixed constant, independent of time and of the local surface structure. The clusters start with zero radius at the time of nucleation, and expand with a radial speed v that is independent of radius. The linear dimension of the section is l.

This method produces values of Δt that satisfy a Poisson distribution with an average value of $(Jl^2)^{-1}$.

The nucleation event is recorded in a list that is subdivided according to the layer in which the event is located. The x and y coordinates of each new event are compared with those for previous events to determine whether the cluster from the earlier event has expanded to cover the point. This comparison is performed starting with the clusters at the highest level, and proceding down to the lower levels. If a cluster is found that satisfies this condition, the new event is assigned to the next level above, and the process is repeated. Otherwise the event is located in the first layer above the substrate.

The natural time unit for the simulation process is $T_1 = (Jl^2)^{-1}$, but for purposes of comparison with models of the infinite system we convert this to the unit $T_2 = (Jv^2)^{-1/3}$, and use the variable $\tau = t/T_2$.

The average growth rates measured at intervals during the deposition of the first four layers are shown in fig. 1. The interface position was measured 100 times during the run, and the square symbols are the average deposition rates during the intervals between measurements.

The Ising model of the crystal-fluid interface can exhibit a number of different growth mechanisms [18–22]. At low temperatures growth on low-index faces appears to have all of the characteristics of 2D nucleation and growth as described by the PNG model. Clusters of atoms form at different locations on the surface and expand and merge with one another to produce new layers.

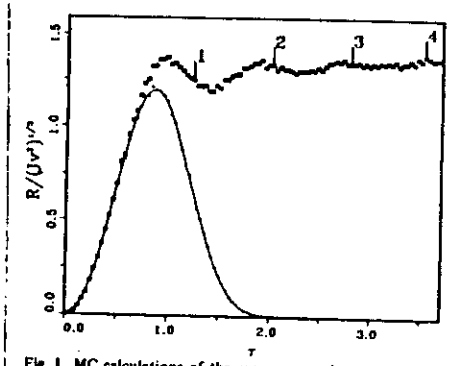

Fig. 1. MC calculations of the average growth rates are plotted versus the dimensionless time τ. The crosses correspond to the rate of deposition in the first layer, and the squares represent the multilevel rate R. The curve is a plot of eq. (7).

The solid-on-solid (SOS) limit of the Ising model of the simple cubic (100) face is used in all of the calculations. This model includes nearest-neighbor bonds of energy ϕ, and the atoms are required to occupy sites of a rigid lattice. The SOS restriction requires that every occupied site be located directly above another occupied site, thus excluding overhangs in the interface and vacancies in the bulk of the crystal. The SOS interface configurations are represented as a square array of column variables $\{h_{11}, h_{12}, ..., h_{ij}, ..., h_{NN}\}$ with discrete heights h_{ij} to indicate the highest level occupied. The physical processes of impingement and evaporation are represented as a unit increase or decrease in the height of a column, i.e.,

$$\{h_{11}, h_{12}, ..., h_{ij}, ..., h_{NN}\} \rightarrow \{h_{11}, h_{12}, ..., h_{ij} \pm 1, ..., h_{NN}\} . \quad (15)$$

Impingement occurs at a rate k^+ that is independent of configuration, but the evaporation rate depends on the number of nearest neighbors n of the atoms:

$$k_n^- = k^+ \exp[-\beta\Delta\mu - (n-3)\beta\phi] , \quad (16)$$

where β is the reciprocal of Boltzmann's constant times the temperature and $\Delta\mu$ is the chemical potential driving force for crystallization. These transition probabilities are consistent with the correct SOS equilibrium partition function when $\Delta\mu = 0$ [24].

A Monte Carlo method is employed to calculate the crystal growth rates. The array of columns is described by a square array of integers. Particular columns are selected by a random number generator, and the process of impingement or evaporation is selected with the appropriate probability using another random number which is compared with a constant that is determined by eq. (16). (See ref. [20] for details).

First we consider the formation of the first layer above the substrate in the case where deposition on higher layers is excluded. The rate of filling of this layer dc_1/dt is shown in fig. 3.

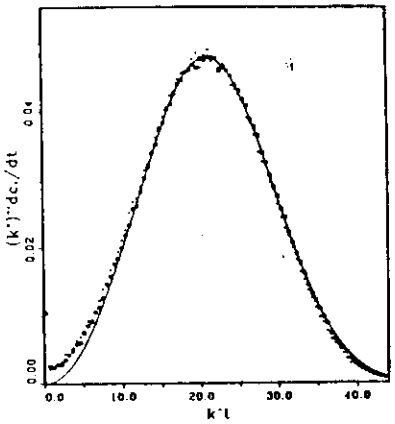

Fig. 3. The rate dc_1/dt is plotted versus time. Monolayer Ising model data are indicated by the crosses and squares for the 40 × 40 and 60 × 60 systems, respectively. Here $\beta\phi$ = 0.25 and $\beta\Delta\mu$ = 2.0. The curve is a plot of eq. (7).

The growth rates of 40 × 40 and 60 × 60 systems (with periodic boundary conditions) are indicated by the crosses and square symbols, respectively.

The two models are also consistent for most of the time period shown. The Ising data tend to fall slightly below the PNG curve at large times; this effect is most pronounced in the 40 × 40 data, and it is apparently a result of finite system size. But the greatest discrepancy occurs in the early part of the transient, where the Ising model rates are much larger than those of the PNG model.

The multilevel transient is shown in fig. 4. The Ising model data are marked by the square symbols. The PNG MC data are also plotted (as crosses) using the same scale factor as in fig. 3. The best fit occurs during the initial rise, since this is the region where the first layer, which was used to obtain the scale factor, dominates the deposition process. The fact that the PNG model predicts a larger rate at the later times may indicate that a higher density of steps (or cluster edges) is achieved. Certainly the steps may be arbitrarily close together without interacting with one another. This is possible since the edges are mathematical lines in the PNG model, whereas they occupy at least one lattice spacing in the Ising model. Furthermore, adjacent steps of the same sign tend to repel one another in the Ising model as a result of a tendency toward irregular step edge configurations and the ability of the step to wander back and fourth with statistical fluctuations [26]. This repulsion would tend to inhibit the formation of regions of high step density in this model, whereas the PNG model has no such effect.

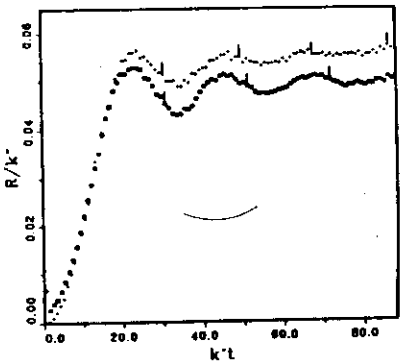

Fig. 4. The total deposition rate R/k^+ is plotted versus k^+t. Squares correspond to the Ising model data, and crosses to the scaled PNG data (see text). Here $\beta\phi$ = 0.25 and $\beta\Delta\mu$ = 2.0.

In order to test the sensitivity of the growth transient to the roughening transition, we have performed calculations at two different temperatures near T_R: kT/ϕ = 0.50, and kT/ϕ = 0.62. The second temperature is equal to a recent estimate of T_R based on extensive MC data [29].

The transients for kT/ϕ = 0.50 are shown in fig. 5. The square symbols give the multilevel rate R, and the triangles indicate the rate in a system constrained to one layer. Qualitatively, the transient growth rates have much the same form as those calculated at half this temperature in the preceding section. But at the lower temperature the first minimum is quite deep, and the amplitude of the subsequent oscillations is significantly larger. The driving force $\beta\Delta\mu$ = 0.4 in fig. 5 results in approximately the same asymptotic growth rate as previously obtained with $\beta\Delta\mu$ = 2.

The equilibrium surface at kT/ϕ = 0.5 includes numerous clusters of adatoms, some containing twenty to thirty atoms. When the driving force is

applied, many of these clusters are already larger than the critical nucleus, and readily expand. These clusters account for the rather large growth rate at the first minimum. At the lower temperature investigated in the previous section, a few individual adatoms were present in equilibrium, but there were very few clusters large enough to be stable in the presence of the driving force. In that case the growth rate remained very small until a few clusters nucleated and grew to a significant size.

Growth transients at the estimated roughening temperature are illustrated in fig. 6. A lower driving force, $\beta\Delta\mu = 0.2$ was chosen to give approximately the same growth rate as in the previous examples. The multi-level rate (square symbols) approaches the constant asymptotic rate in a very short time, after only a fraction of a monolayer has been deposited. Apparently the only time-dependent effect is an initial surge in the concentration of adatoms and small clusters, and these produce the rapid decay from a large initial rate just after the driving force is applied. The transient in a system restricted to a monolayer (triangles) is also appreciably different from the curves measured below T_R. In this case a monotonic decrease in the growth rate is observed. It is apparent from these results that the process of growth has little relation to the degree of completion of the various layers of the crystal. This is in accord with our picture of the interface above T_R, where large clusters cause the interface to fluctuate in the vertical direction with no barrier to its motion from one level to the next.

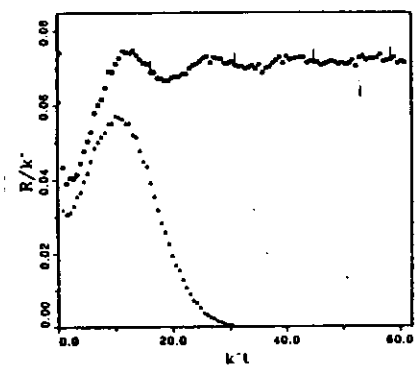

Fig. 5. The Ising model monolayer deposition rate dc_1/dt and the total rate R are plotted versus k^2t as triangles and squares, respectively. Here $\beta\phi = 0.50$ and $\beta\Delta\mu = 0.4$.

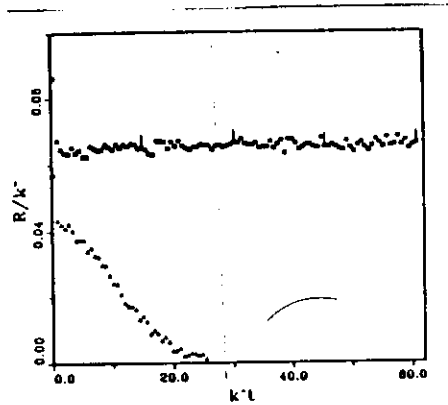

Fig. 6. The Ising model monolayer deposition rate dc_1/dt and the total rate R are plotted versus k^2t as triangles and squares, respectively. Here $\beta\phi = 0.62$ and $\beta\Delta\mu = 0.2$.

CHAPTER III

GAS - SURFACE INTERACTIONS

INTRODUCTION

Historically, atomistic theories[1] of crystal growth on an atomically perfect surface are based upon model considerations of an elemental solid grown from atomic vapor, and have served well to expose the relative role of surface migration and evaporation kinetics in establishing the widely used concepts of nucleation and continuous-growth mechanisms of growth initiation.[1,2] A majority of vapor-phase crystal growth, such as molecular-beam epitaxy[3] (MBE) of III-V compounds, however, involves at least one species in molecular form leading to surface molecular reactions as integral kinetic steps during growth—a feature whose significance for the growth-initiation mechanism and the nature of the nonequilibrium surface has not been previously examined. Studies of the kinetics of [100] MBE growth of GaAs have established[4,5] that under the As-stabilized surface-growth conditions normally employed, (a) the crystal growth rate is controlled by the group-III (i.e., Ga) flux whose incorporation rate is unity and (b) the growth is kinetically controlled by the adsorption kinetics of the molecular group-V species. The atomistic nature of the MBE growth-initiation mechanism has not been experimentally established even though assertions abound that it is the two-dimensional nucleation mechanism. Historically, the term nucleation mechanism of growth initiation has been used to refer to a process in which diffusion-limited formation of clusters stable against breakup to the parent phase is a necessary requirement for the growth to occur. In the literature of vapor-phase crystal growth, the parent phase has conventionally been taken to be the vapor. The unity incorporation rate of the growth-rate–controlling group-III atoms under the usual conditions employed thus indicates that this conventional view of a nucleation process from the vapor is not operative in MBE. In an effort to shed light on what atomistic processes might be involved, and under what kinetic conditions, here we present some results of the first Monte Carlo (MC) computer simulations based upon a model which accounts for (a) and (b) above and examines the role of the surface molecular-reaction kinetics in influencing the growth process. It is found to lead to a more general growth process, referred to here as a configuration-dependent, reactive-incorporation (CDRI) growth process, which also includes the conventional nucleation or continuous-growth mechanisms as special cases, realized under appropriate kinetic conditions.

INTERACTION KINETICS OF As WITH Ga

As_4 molecules

temperature regime 300°K to 450°K

In the absence of a Ga adatom population, there was no measurable sticking coefficient of As_4 on {100} oriented GaAs substrates, i.e. there was no frequency independent attenuation of the signal from desorbed As_4. Previous observations [1,2] that the sticking coefficient of Ga in this temperature range was unity and independent of surface composition were also confirmed. When a modulated As_4 beam and an unmodulated Ga beam impinged simultaneously on a substrate, a temperature dependent sticking coefficient of As_4 (S_{As_4}) was measured, approaching unity at the lower temperatures, as shown in fig. 2.

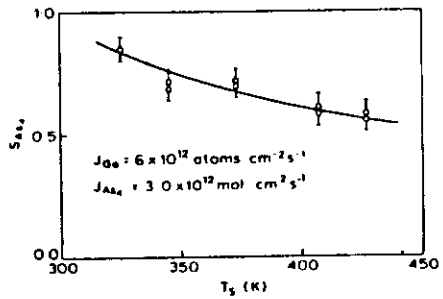

Fig. 2. Sticking coefficient of As_4 on {100} GaAs in the presence of a Ga beam, as a function of temperature below 450 K.

In general terms the results indicate that there are two basically different mechanisms for the interaction of As_4 and Ga on GaAs surfaces, one below ~ 450 K, and one above. The behaviour in the low temperature region would seem to correspond to simple non-dissociative chemisorption of As_4 molecules onto Ga atoms on the surface of GaAs, via a precursor state. In the absence of surface Ga atoms only physisorption occurs. The evidence for this may be summarised as follows:

(i) All desorbed As_4 molecules have completely thermally accommodated with the surface, and there is a measurable surface lifetime with an activation energy for desorption (0.38 eV) which is commensurate with desorption from a weakly bound precursor state. In the presence of a Ga adatom population, where the sticking coefficient for As_4 becomes non-zero, the desorption energy obtained from lifetime measurements remains the same as when S_{As_4} is zero, only the pre-exponential factor changes. This implies that desorption always occurs from the same binding state.

(ii) All As_4 desorption processes follow first order kinetics.

(iii) The As_4 sticking coefficient in the presence of surface Ga atoms tends to unity and increases with decreasing temperature.

(iv) Examination of desorbed species shows no evidence of dissociation.

The region 450–600 K

Over this range S_{Ga} was always unity, in accordance with previous experiments [1,2] and the surface lifetime of As_4 was too short to measure, i.e. $< 5 \times 10^{-5}$ sec. In the absence of a surface concentration of Ga, S_{As_4} was zero, but by impinging an unmodulated Ga beam with the modulated As_4 beam the results shown in fig. 3 were obtained. From this it is clear that S_{As_4} assumes a finite value in the presence of a Ga beam, but that it is independent of temperature over the whole range. The direction of temperature change during the course of an experiment in which fluxes of As_4 and Ga were kept constant did not affect the results, and the reproducibility was also much better than in the lower temperature region.

Although S_{As_4} is temperature independent, fig. 3 also shows that there is a strong dependence on the flux of Ga atoms, J_{Ga}, to the surface. The results are plotted in fig. 4 to indicate the form of this dependence, together with additional data points obtained by varying the Ga flux at two fixed substrate temperatures (455 and 575 K), showing that the method of performing the experiment (i.e. varying either J_{Ga} or T_S) did not affect the result.

In addition to the temperature independence of S_{As_4}, three other factors emerging from these results need to be emphasised. The first is that under no conditions did S_{As_4} exceed 0.5, even when the Ga flux far exceeded the As_4 flux. This is to be contrasted to the behaviour below 450 K, where S_{As_4} tended to unity.

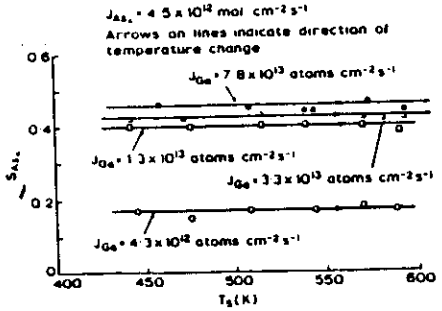

Fig. 3. Sticking coefficient of As_4 on {100} GaAs as a function of temperature between 450 K and 600 K for various Ga beam fluxes.

The final stage is to attempt to deduce a mechanism for the interaction of As_4 and Ga on {100} GaAs surfaces at temperatures > 450 K from the kinetic results presented in section 3. In constructing any model several important factors must be taken into account:

(i) The sticking coefficient of As_4 is always ≤ 0.5, irrespective of the Ga flux, and As_4 adsorption is non-activated ($S_{As_4} \neq f(T)$).

(ii) When there is an excess of arsenic, each Ga atom supplied consumes one As atom.

(iii) Any Ga supplied which is in excess of that producing the maximum value of 0.5 for S_{As_4} is eventually consumed if an As_4 beam is maintained after the Ga beam is turned off.

(iv) The order of the desorption process with respect to As_4 changes from second at low As_4 coverages (relative to the Ga coverage) to first at high coverages.

(v) There is no measurable desorption of As_2 (or any species other than As_4) below 600 K.

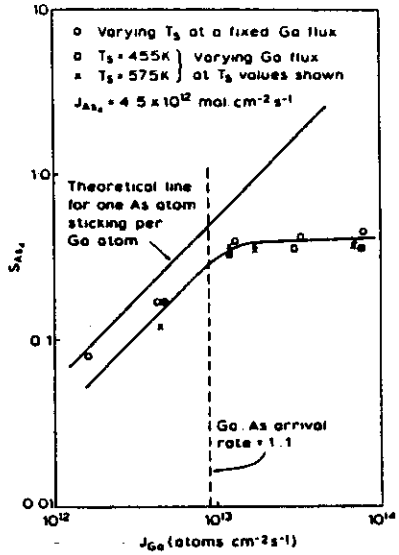

Fig. 4. Sticking coefficient of As_4 as a function of Ga beam flux in the temperature range 450–600 K.

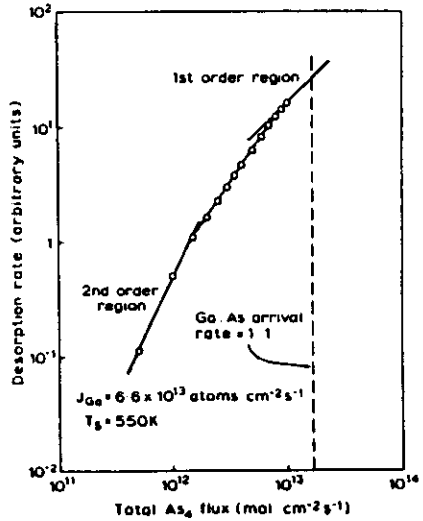

Fig. 5. Reaction order for As_4 desorption with respect to the As_4 flux to the surface of {100} GaAs in the presence of a constant Ga flux for a substrate temperature of 550 K.

The fact that there is a region where desorption kinetics are second order and that S_{As_4} never exceeds 0.5 implies that chemisorption must be dissociative, with a pairwise, rather than a single As_4 molecule interaction with Ga sites.

$$As_4(\text{vapour}) \longrightarrow As_4^* \text{ (precursor)}$$

$$As_4^* + As_4^* \longrightarrow As_2^* + As_2^* + As_4(\text{vapour})$$

As_2 molecule

The first series of experiments was concerned with determining the nature and relative intensities of species desorbing from the {100} oriented GaAs substrate as a function of its temperature, for an incident As_2 flux, but without a separate Ga beam. The measurements were made by examining the response of the mass spectrometer while modulating the desorption flux, with an unmodulated As_2 incident intensity of 10^{13} molecules $cm^{-2}\ s^{-1}$. The results are illustrated in fig. 2, the most important feature being that below ~600 K an association reaction occurs, with the formation of As_4. There is a consequent decrease in the desorption rate of As_2 below 600 K, while at higher temperatures it remains constant. The decrease in the As_4 desorption rate below ~450 K is probably associated with the non-dissociative chemisorption of As_4, which is formed on the surface, on to those Ga atoms

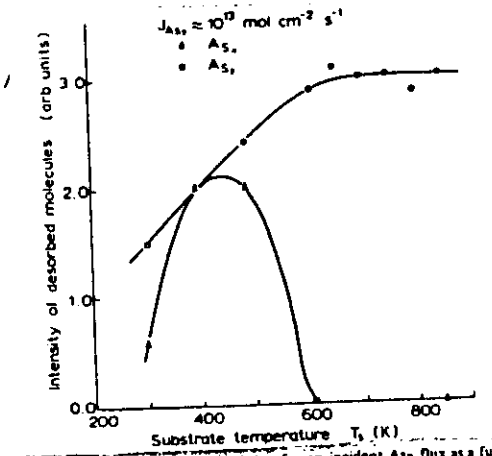

Fig. 2. Relative desorption rates of As_2 and As_4 for an incident As_2 flux as a function of substrate temperature.

which arrive with the incident As_2 beam. This type of chemisorption is precisely the same as that observed [9] when beams of As_4 and Ga are directly incident in this temperature region, with the As_4 sticking coefficient approaching unity at ~300 K if there is a sufficiently high Ga adatom population.

The sticking coefficient of As_2 was also measured at a substrate temperature of 600 K in the presence of an incident flux of Ga. As explained above, both the association reaction and the rate of formation of a Ga adatom population by evaporation of As_2 are negligible at this temperature, and this therefore corresponds to the least complex interaction behaviour. The results are shown in fig. 5, the important point being that S_{As_2} tends to unity, compared to the asymptotic value of 0.5 for As_4 under similar conditions [9]. For comparatively low Ga fluxes, S_{As_2} is also directly proportional to the Ga flux, and within experimental accuracy each Ga atom supplied interacts with one As atom (for low Ga fluxed). At higher fluxes, the excess Ga probably accumulates on the surface.

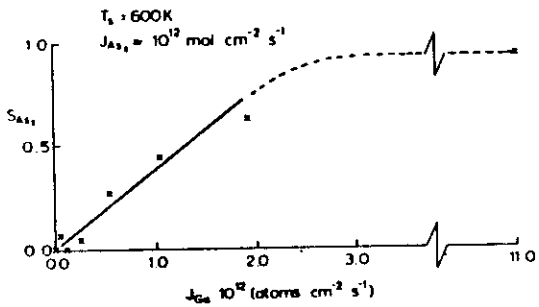

Fig. 5. Sticking coefficient of As_2 on a {100} GaAs surface at 600 K as a function of the Ga flux.

Having proposed this qualitative description, the next stage is to attempt to model the reaction sequence so that we can predict the phase and amplitude behaviour of the measured signal in terms of surface processes. It will be convenient to treat separately the reaction sequences above and below 600 K. Consider first the high temperature case, where the experimental result is an attenuation of the As_2 signal with respect to a modulated incident As_2 flux, independent of frequency over a wide range. The basic reaction steps can be represented by eqs. (1):

$$\begin{array}{l} \xrightarrow{J_{As_2}} As_2(p) \xrightarrow{+\text{ Ga atom pair},\ k_2} (As + As)(c) \\ \qquad\qquad \downarrow k_1 \\ \qquad\qquad As_2(v) \xleftarrow{k_3} \end{array} \qquad (1)$$

The nomenclature used in these equations is as follows: J_{As_2} is the incident As_2 flux, (p) represents a precursor state on the surface, (c) a chemisorbed state and (v) a vapour phase state. The terms k_i are rate constants for the various reactions.

We can now consider reaction sequences which occur on the surface below 600 K, where the basic steps are represented by eqs. (9) below:

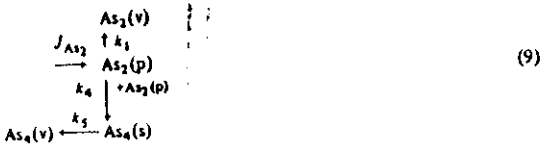

(9)

All symbols have the same meaning as before, and in addition (s) refers to a surface molecule.

ATOMISTIC MODEL, INPUT RATE PARAMETERS AND COMPUTATIONAL CONSIDERATIONS:

(IV.A) The Generic Model:

Employing the kinetic studies of Arthur[17,19] and of Foxon and Joyce[21-23] as a guideline, Singh and Madhukar began the first efforts[5,6] at constructing an atomistic model which may serve as a starting point towards computer simulations of MBE growth. The present status of the level of atomistic detail included in the models themselves, as well as the degree of numerical sophistication of the simulation process have both evolved[6-15,30,32] rapidly and considerably from these early beginnings. This section presents the essential features of the atomistic model via the example of GaAs growth on As-stabilized GaAs(100) surface. The relevance of all the essential features embodied to other binary III-V compounds grown on a lattice matched substrate will be self evident.

The first feature of the models is that they consider an ideal, unreconstructed, GaAs(100) surface terminating with As atomic plane and represented by an (NXN) square lattice of sites (i,j). The size N has been taken to be from 30 to 100 depending upon the particular issue to be examined. Similarly, the thickness of the layer grown in the

simulations has varied from a few atomic layers to up to 30 atomic layers. We postpone a discussion of the choice of substrate size and the obvious related issue of reliability and accuracy of the simulations to section IV(C). Note that the absence of an explicit presence of surface reconstruction automatically implies that the energetics and kinetic processes associated with un-reconstructing the surface locally around the site where a Ga or As atom is eventually epitaxially incorporated is not explicitly a part of the simulations carried out to date. Some of the associated effects, however, may be implicitly understood to be included in the choice of particular kinetic rates, as will be seen.

The second basic feature of the model is that the interactions amongst and between the group III and group V atoms (hereafter referred to as cations (C) and anions (A), respectively) are effectively thought of as being short ranged and represented through phenomenological interaction energies, V_{A-C}, V_{C-C} and V_{A-A} for the unlike nearest neighbors and like nearest neighbors. The tetrahedral nature of the III-V semiconductor is explicitly accounted for so that the interaction terms retained correspond to the nearest and second nearest neighbor interactions of the compound semiconductor. Thus V_{A-C} represents the interaction energy for the sp^3 hybrids of Ga and As bonding with each other. The total bonding energy of a given cation is thus $(nV_{A-C} + mV_{C-C})$ where n and m represent the number of cation-anion nearest neighbor bonds and cation-cation second nearest neighbor bonds formed at the instant of time of interest. For n=4 and m=12 the atom is assumed to be fully coordinated. The corresponding total bonding energy is assumed to be nearly the same as the heat of formation of the solid. Approximate as it may be, this prescription provides a guide line for choosing V_{A-C}, V_{A-A} and V_{C-C}, as well as, for scaling these interactions from one compound to another, including lattice matched pseudobinary alloys of the type III-III-V (e.g. $Al_xGa_{1-x}As$ on GaAs).

The third feature of the models is that they account for the group V species being initially in a weakly adsorbed As_2^* state. This is the appropriate starting point when an As_2 vapour flux is employed, as discussed in the previous section. When an As_4 vapour flux is employed, this would be an appropriate starting point only for growth conditions for which generation of the As_2^* species from the As_4 vapour is not the rate limiting step in growth. For the usual growth conditions employed in MBE of GaAs, this has also been seen in the preceding section to be the likely case. The surface population of the As_2^* species during growth (denoted by $N_{As_2^*}$) is a function of the substrate temperature, Ga flux, and As_2 (or As_4) flux through the behaviour of the sticking coefficient of As_2 (or As_4). In the case of As_4, the surface migration of the intermediate $As_4(c)$ species postulated by Foxon and Joyce, as well as the reaction rate constant, $K_{As_4}(c)$, will naturally also influence the steady state As_2^* population. In either case, the models further assume growth conditions such that availability of the As_2^* surface species is not the rate limiting step.

The fourth important consideration of the models is in fact the first encounter with atomistic detail. This has to do with the Ga atom configurations of primary significance to the dissociative chemisorption reaction pathways available to the As_2^* specie.

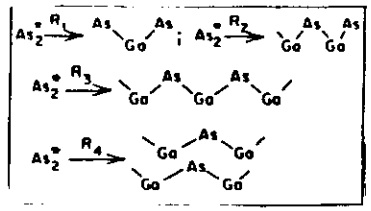

The dissociative chemisorption reaction of As_2 from a precursor physisorbed state, As_2^*, has been suggested[4,5] to require two unfilled As sites on the surface, although the specific nature of these sites could not be established. We thus consider the lowest-order Ga configurations capable of providing a pair of adjacent unfilled As sites. These are a single Ga, two adjacent Ga atoms along the bond orbital direction, three consecutive Ga atoms along the bond orbital direction, and four Ga atoms in the surface nearest-neighbor square configuration (Fig. 1). We denote the kinetic rates for As_2^* dissociative incorporation via these reaction pathways as R_i, $i = 1$–4, respectively. The atomic Ga is allowed to bind with single or two adjacent As atoms with a sticking probability of unity, thus creating a single Ga—As or a double Ga—As bond.

In addition to the intra-planar Ga atom configurations, configurations involving Ga atoms in two different (100) planes, such as would occur at steps, can also provide sites for As_2^* dissociative reaction. A few such configurations are shown in fig. 4-2. Besides the nearest interplanar Ga neighbor configurations, one may also have configurations involving higher nearest neighbors of the tetrahedral structure. This may suggest that the rate constants for reactions occuring at such steps may be lower than the other inter- and intra-planar configurations. On the other hand, the high asymmetry of the charge distributions at the steps may give rise to potential energy surfaces such that the activation energy for the reaction rates along certain directions in the free energy-configuration coordinate diagrams may, in fact, be lower in spite of the larger separation of the interplanar Ga atoms. No information on such matters is presently available.

In appreciating the relevance of the intra and inter planar Ga configurations and their associated rate constants, $K_i(T)$, for the dissociative chemisorption reaction of As_2^*, two equally important additional kinetic aspects must be clearly recognized.[11,13-15] The first is the steady state population of As_2^* at the surface which depends upon the chosen As_2 or As_4 vapour flux, the Ga vapour flux and the substrate temperature through the As_2 (or As_4) adsorption and As_2^* desorption kinetics. Let us denote such a steady state population by $N_{As_2^*}(T_s, P_{As_4}, F_{Ga})$. The second is the probability, P_i, of occurrence of the i^{th} Ga atom intra or interplanar configuration. Under the usual GaAs growth conditions the sticking coefficient of Ga is unity. The probabilities P_i are thus a function of time through both, the arrival rate of Ga (the Ga flux, F_{Ga}) and the surface migration rates, $h_\alpha(T)$, for the Ga atoms in the α^{th} chemical bonding state. We discuss the migration rates later in this section, but for the moment let us denote the probabilities by $P_i(t, \{h_\alpha(T)\}, F_{Ga})$. Then, the quantity of interest to the growth of the GaAs solid phase being the *incorporation rate* of Ga and As from the vapour, it is readily realized that the latter is achieved through the collective role of each of the different Ga configurations at

rates given by the product,

$$N_{As_2^*}(T, P_{As_4}, F_{Ga}).K_i(T).P_i(t,\{h_\alpha(T)\}, F_{Ga}) \qquad \text{(IV.1)}$$

Several important features of the growth process are revealed by expression (IV.1). First, it is seen that the relative significance of the various Ga atom configurations changes with time during the growth of a given layer due to the time dependent change in the P_i's. Second, an explicit As_2 or As_4 vapour pressure dependence is seen to enter[13,15] through $N_{As_2^*}$. Third, an implicit dependence on the local environment dependent Ga hopping rates (both intra and interlayer), $\{h_\alpha(T)\}$, is seen to be present. Equally important, to the extent that the time evolution of P_i depends, at least in the initial states of growth of a given Ga layer, on the hopping rates $h_\alpha(t)$ where α represents the chemical bonding states for the Ga atoms, and to the extent that a change in the bonding state of a given Ga is affected by expression (IV.1) defining the incorporation of the As atoms, the life time of the Ga atoms in the i^{th} configuration is itself influenced by $K_i(T)$ and $N_{As_2^*}$. Since it is always the product of a kinetic rate and the time that it is operative that is of physical significance, it is also recognized that the "effective" migration ability[14,15] of the Ga atoms is itself dependent upon the reaction rate constants $K_i(T)$ as well as the As_2(or As_4) vapour pressure through the steady state population, $N_{As_2^*}$. Thus a significant arsenic pressure dependence[13,15] of the growth process and surface morphology can be expected under many growth conditions (i.e. choice of T_s and F_{Ga}).

The relevant time scale for the operation of a given kinetic process, such as the surface migration rates $h_\alpha(T)$, is seen to be the life time τ_α which is dependent upon the Ga flux, the reaction rate constant $K_\alpha(T)$ and, of course, $N_{As_2^*}$. Thus we may recognize τ_α to be a function of these three quantities by writing it as $\tau_\alpha(P_{As_4}, K_\alpha(T), F_{Ga})$. Assuming the average surface residence time of the Ga atoms to be longer than τ_α (for otherwise growth of the solid would be most unlikely), the effective distance, ℓ_α, moved by the Ga atom in state α is of order $(h_\alpha(T).\ \tau_\alpha)^{1/2}$, in units of the nearest surface neighbor

distance.[5] The overall range sampled by the atom prior to its incorporation is then some appropriate average of ℓ_α over all α. Let us denote it by $\ell_{eff} \sim <\Sigma_\alpha\ (h_\alpha(T)\tau_\alpha (P_{As_4}.K_\alpha(T).F_{Ga}))^{1/2}>$. One sees that the effective migration length is a function of the three user controlled growth parameters – T_s, P_{As_4} and F_{Ga}. Thus, for a given choice of these parameters, ℓ_{eff} may or may not be greater than W_o, the average terrace width of the starting substrate. For growth conditions such that $\ell_{eff} < W_o$, the growth initiation process would involve predominantly addition of material on the terraces as has been discussed in section II. The atomistic mechanism of growth initiation, however, need not be the conventional nucleation and growth mechanism of section II, as will be seen in the following. Note that within the simulation model, choice of an (NXN) substrate with no steps in it is equivalent to restricting the simulations to growth on the terraces of a real substrate, i.e. $l_{eff} < W_o$. Periodic boundary conditions on the (NXN) substrate are employed to avoid edge effects and the convergence of the results tested against the size N.

The expression (IV.1) representing the incorporation rate of arsenic also reveals the significant role that the As_2^* reaction rate constants $K_i(T)$ can play in governing the atomistic nature of the MBE growth mechanisms. The possibility that the reaction rate constants $K_i(T)$ may become the rate limiting step for arsenic incorporation under certain growth conditions is self evident. There is no analogue of this behaviour in the historical atomistic models and computer simulations summarized in section II. Thus even though the *time averaged* growth rate of GaAs may be controlled by the arrival rate of the Ga under a sufficient population of As_2^*, the *time dependent* growth rate can be controlled by the reactive incorporation kinetics of the As_2 molecules, consistent with the kinetic studies of Arthur summarized in section III. Ghaisas and Madhukar (GM) have thus termed[11,13,14] such a generic growth process a Configuration Dependent Reactive Incorporation (CDRI) process. At one extreme of the CDRI process is the time dependent

growth rate behavior controlled by the As_2^* dissociative incorporation rates. GM have shown[11,14] this to be a possibility and called such growth mechanism the Reaction Limited Incorporation (RLI) growth mechanism. On the opposite extreme is also the possibility that the incorporation kinetics of the arsenic is limited by the Ga configuration probabilities, P_i, and not either by $N_{As_2^*}$ or by the reaction rate constants, $K_i(T)$. Growth conditions giving rise to such a situation have also been examined by GM and has been referred to as the Configuration Limited Reactive Incorporation (CLRI) growth mechanism.[11,14]

The preceding discussion of the Ga-configuration dependent reactive incorporation of arsenic and its possible consequences expected to manifest themselves as the new RLI and CLRI growth mechanisms is relevant to the regime of a unity sticking coefficient of Ga (S_{Ga}). Recall that the operational definition of S_{Ga} being used in this review is the same as the incorporation rate of Ga. The situation considered hitherto thus corresponds to an effectively negligible Ga evaporation rate. The atomistic CDRI model of Ghaisas and Madhukar, however, is not limited to near zero evaporation rate of Ga atoms and is fully capable of describing the growth process under conditions where the Ga evaporation rate may become significant. Under such conditions the incorporation rate of Ga from the vapour phase into the GaAs solid phase would be less than unity. The growth mechanism should then become very similar to, if not the same as, the conventional notion of nucleation and growth mechanism of growth initiation on flat terraces discussed in section II. Let us therefore examine the nature of the Ga evaporation process.

As should be clear by now, the MBE growth process of III-V semiconductors occurs under very far from thermodynamic equilibrium conditions. Consequently, it is the individual desorption rates of the Ga atom from its various bonding configurations which need to be explicitly considered in the atomistic simulations. Approximations such as inherent in the Wilson-Frenkel description of section II which approximates the effective

evaporation rate of atoms during growth to be that from the kink sites at thermodynamic equilibrium, though employed[10] by Singh and Bajaj, have little chance of being valid even at the high temperatures where, for elemental solids, it may be a reasonable approximation. Similarly, mean field type of approximations, such as inherent in the Temkin theory of section II, are of no value. The compound nature of the III–V semiconductors involves a dependence of the evaporation behaviour of one specie on that of the other, particularly under the far from equilibrium conditions operative in MBE. Even the usual notion of the congruent temperature (T_G) is not applicable to a free compound solid surface at vapour pressures significantly far from equilibrium, even though T_G is a useful reference point for guiding one's thinking. In the atomistic model[11,15] of Ghaisas and Madhukar, neither are such approximations made nor are they necessary. The only assumptions made are, (i) that thermodynamic equilibrium exists between the desorbing atom and its local environment on the solid so that it experiences a temperature which is the same as the substrate temperature, and (ii) that an Arrhenius expression involving a local bonding configuration dependent activation energy and prefactor represents well the desorption rate of the Ga atom from that local bonding configuration. With these assumptions, the local configuration dependent Ga evaporation rates are taken to be,

$$R_E^i(T) = R_{OE}^i \exp(-E_A^i/k_BT) \qquad \text{(IV.2)}$$

where i denotes the i^{th} configuration. The prefactors R_{OE}^i and the activation energies E_A^i for each of these local configuration dependent desorption rates need to be ascertained. It is important to recognize that experimental information on overall evaporation rates can at best be employed as a judicious guide to the expected range of values for R_{OE}^i and E_A^i since it is the collective consequence of R_E^i for all I which is typically available in the form of evaporation rates. It is generally thought reasonable to identify the activation energy in a desorption rate with the total binding energy, E_{Tot}^i of the particle. This is, however, true at best when the desorption process occurs directly from the particular state under consideration, without involving intermediate states. For the group III atoms thus it would be reasonable to assume that $E_A^i = E_{Tot}^i$ but for the group V atoms the binding energy in the atomic chemisorbed phase is not the relevant activation energy since desorption occurs from a molecular state. The atomistic models thus employ the following expression for the group III atom desorption rates:

$$R_E^i(T) = R_{OE}^i \exp(-E_{Tot}^i/k_BT) \qquad \text{(IV.3)}$$

Finally, we discuss the surface migration rates. In the preceding discussion, for simplicity, we employed the short hand notation, $h_\alpha(T)$, to denote the hopping rate from a given chemical state, α. Here we discuss the nature of these rates in some detail.

Just as for the adsorption rates, reaction rates and desorption rates, it may further be reasonable to assume equilibrium between the initial and final configuration with an activated state involved in the migration process. The absolute rate theory would then, once again, suggest that an Arrhenius form for the surface migration rates would be a reasonable expectation. As such, the jump rates may be written as,

$$h_{\alpha\alpha'}^{m,n}(T) = h_{o\alpha}\exp(-E_{\alpha,\alpha'}^{A}(m,n)/k_BT) \qquad \text{(IV.4)}$$

where (α,m) represents the initial state (α) and site (m) and (α',n) the final state (α') and site (n) to which the jump is made. Within the absolute rate theory approximation, the prefactor would depend only upon the initial configuration. The activation energy, however, can depend significantly upon both the initial and final configuration, the separation between the sites, and the direction of the jump. It is the precise nature of the potential energy surface as a function of the "configuration coordinates" between the initial and final states (the term state here representing both chemical state and configuration) which will determine the behavior of the activation energies involved.

The nearest intra and inter planar Ga neighbor hopping rates at the surface have been taken to be of an Arrhenius form and parameterised as,

$$h_i^{II}(T) = h_{oi}^{II} \exp\{-(E_i^{Tot} - \Delta_i^{II})/k_B T\}$$

$$h_i^{I}(T) = h_{oi}^{I} \exp\{-(E_i^{Tot} - \Delta_i^{I})/k_B T\} \quad \text{(IV.5)}$$

where i denotes the configuration from which the hop is made, II and I denote intra and interplanar hop, h_{oi}^{II} and h_{oi}^{I} are the corresponding prefactors, E_i^{Tot} is the total binding energy (within the second bulk nearest neighbor approximation inherent in the model) of the Ga atom in the i^{th} configuration, and Δ_i^{II} and Δ_i^{I} are parameters which may be adjusted to define the corresponding activation energies as $(E_i^{Tot} - \Delta_i^{II})$ and $(E_i^{Tot} - \Delta_i^{I})$.

To the extent that it is the incorporation rate (and not the reaction rate alone) which enters the crystal growth process, we may model the absolute and relative behavior of the products of $N_{As_2}^{*}$ and $K_i(T)$. Denoting these products as R_i, we then recognize that these rates are a function of both temperature and group V pressure: $R_i \equiv R_i(T, P_{As_4})$. Ghaisas and Madhukar take this approach and specify R_i, $i \neq 1$, in terms of R_1 which itself is then varied as a parameter.[13,15]

SIMULATION

In the work of Ghaisas and Madhukar, the time of occurrence of a particular kinetic event for a given particle is determined via,

$$\tau = -\frac{1}{R} \ln Z \quad \text{(IV.8)}$$

where R is the corresponding rate parameter and Z a random number. The random number Z is taken to be distributed, with a uniform probability, between 0 and 1. Expression (IV.8) thus defines a Poisson distribution of the time, with a mean value given by the inverse of the rate. The simulation process then begins with the arrival of a given group III atom at a site (i,j) chosen randomly with equal probability for all sites in the chosen (NXN) As-stabilized (but unreconstructed) surface. The time interval of arrival of the subsequent group III atom from the vapour can also be determined according to a suitable distribution with an average time interval equal to the inverse of the chosen flux. Upon arrival of the first group III atom, the times for each possible kinetic event for the particle (such as hopping, reaction, evaporation) are calculated and ordered according to increasing magnitude. Events, starting with the one with the shortest time interval are allowed to occur until the time for occurence of the next kinetic event exceeds the time for arrival of the next group three atom. Then the next group III atom is allowed to impinge at a site chosen randomly according to the previously noted prescription and including the site(s) occupied by the previously arrived atom(s). If the arrival of a group III atom is within a spatial range which influences any of the previously arrived atoms, then their time clocks for each of the possible kinetic events are reset according to the new applicable rates, and the time of occurence of events for all the particles reordered to begin from the shortest to the longest time interval less than the time of arrival of the next group III atom. The same is, of course, true if between the arrival from the vapour of subsequent group III atom, the occurrence of a given surface kinetic event (such as hopping, for example) for a given atom influences the rates of other kinetic events of either the same atom, or the kinetic rates of other atoms.

With regard to Ga migration, SB improved the simulation model by incorporating[9,10] a limited degree of interlayer Ga migration from sites

Through the use of the parameters Δ_{ll} and Δ_{l} occurring in equn (IV.5), these authors obtained results[10] for GaAs(100) homoepitaxy for two cases – equal intra- and inter-layer Ga hopping rates, and inter-layer hopping rate slower than intra-layer hopping rate. Results were reported[10] for two different substrate temperatures, 700°K and 810°K, which shed light on the role of interlayer migration and helped clarify the deficiency in the initial results[7,8] of Singh and Madhukar in respect to the kinetic roughening phenomenon. In particular, no roughening of the growth front profile with increasing substrate temperature was found in the presence of the interlayer migration. The predominant motivation and thrust of this work of SB reported in references (10) and (12), however, appears to be the desire to examine the nature of the interfaces formed during heteroepitaxy of $Al_xGa_{1-x}As$ on GaAs(100) – the so called normal interface – and of GaAs on $Al_xGa_{1-x}As$, the so called inverted interface.

All simulations have been carried out on substrates of sizes up to 50×50 with periodic boundary conditions to avoid edge effects and to test against convergence, and averaged over ten independent random number sets to obtain accuracy of ±3%. The thickness of the film grown is up to 22 atomic layers. The Ga flux employed is equivalent to delivery of 1.1 monolayer/sec. The substrate temperature is chosen to be 575 °C. The interaction energies for the nearest-neighbor Ga-As and second-nearest-neighbor Ga-Ga interactions are chosen to be 0.7 and 0.1 eV, respectively, which give rise to a total Ga—As bond energy consistent with the heat formation. All the kinetic rates are taken to have the Arrhenius form. the kinetic rates are taken to have the Arrhenius form. The activation energy for hopping of the Ga is defined as the total of Ga-As and Ga-Ga interaction energies minus a parameter Δ which is varied to cover the expected range of Ga surface diffusion. The hopping rates for the singly and doubly bonded Ga are $h_1 = 6614$/sec and $h_2 = 1690$/sec, respectively, which correspond to equivalent diffusion lengths of about 255 and 115 Å—values consistent with the only reported[11] attempt to determine Ga diffusion constant under As-stabilized conditions at 550 °C, but in the absence of growth. During growth, the effective migration distance (l_{eff}) of Ga will be significantly less and, for the results presented here, is significantly less than the matrix size which models the terrace width of a real surface (i.e., the operational definition of an atomically perfect surface). We present results for two sets of values for the As_2 incorporation rates R_1 and R_2—the first for $R_1 = 10$/sec and $R_2 = 20$/sec, and the second $R_1 = 1000$/sec and $R_2 = 2000$/sec. In the latter case, the interlayer cation migration rate is taken to be twice as fast as in the former case. The rates R_3 and R_4 are taken sufficiently high so that the reaction occurs with essentially unit probability once the configuration has occurred.

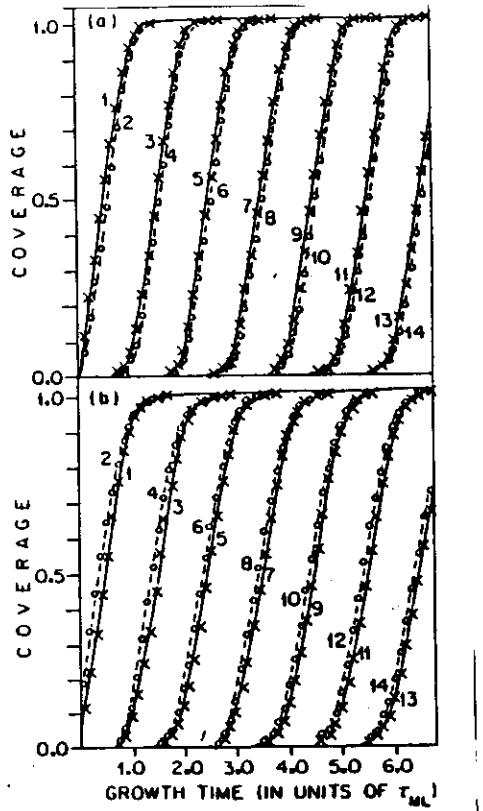

FIG. 1. Coverage buildup in each layer as a function of crystal growth time measured in units of the Ga monolayer delivery time ($\tau_{ML} = 0.9$/sec) for (a) slow and (b) fast reaction rate (R_1) at single Ga sites. The odd- (crosses) and even- (circles) numbered curves indicate the Ga and As layer coverages, respectively.

In Fig. 1(a) is shown the coverage buildup as a function of growth time for the slow incorporation rates. The n = odd layers are Ga whereas n = even layers are As. It is seen that of the first monolayer's (ML) worth of Ga delivered ($\tau_{ML} = 0.9$/sec), almost 95% goes into the first layer and only about 5% into the next Ga layer. This distribution for subsequent arrival of monolayers of Ga changes somewhat before the growth-front profile stabilizes, but still maintaining a layer-by-layer mode of material addition. Note that the slow rates R_1 and R_2 make the As coverage lag behind the immediately preceding Ga layer coverage until the near completion of the layer. The growth front is, however, As-stabilized throughout the growth. In Fig. 1(b) is shown the coverage buildup for the faster incorporation rates R_1 and R_2. Note that while the layer-by-layer mode of addition of material is clearly maintained, coverages of the As layers are seen to lead the coverage of the preceding Ga layers. This is a consequence of the rapid incorporation rate R_1 leading to attachment of essentially two As atoms for each Ga deposited at the initiation of a given layer.

A deeper insight into the mechanism of growth is provided by the growth rate behavior shown in Fig. 2. The Ga attachment rate is constant at the employed Ga flux of 1.1 ML/sec for both slow and fast rates R_1 and R_2. The total growth rate (i.e., Ga+As incorporation rate) measured in units of a bilayer, however, exhibits oscillations in both cases, starting from very low values in the former case (curve *a*) but very high values in the latter (curve *b*). For slow rates R_1 and R_2, the arsenic incoporation rate is low in the initial stages of growth since most of the Ga delivered are mostly in single configuration. With subsequent continued arrival of Ga atoms, two- and higher-Ga configurations begin to occur, both due to the effect of surface migration and increased coverage. Consequently the rates R_2, R_3, and R_4 take over, increasing the incorporation rate of As_2. As a given Ga layer nears completion, even the rapid interlayer Ga migration cannot prevent the next higher Ga layer from being initiated, whence the process of As_2 incorporation repeats itself, giving rise to the observed oscillatory behavior. Such a growth-initiation process may be appropriately referred to as a reaction-limited–incorporation (RLI) growth mechanism. For values of R_1 high and comparable to h_2, as in curve *b*, the As incorporation rate can significantly exceed unity at the earliest stages since for each Ga, essentially two As atoms are incorporated. Subsequently, however, the As incorporation rate must slow down since rapid interlayer

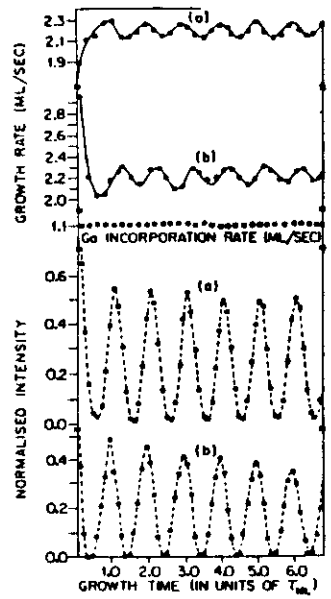

FIG. 2. Ga attachment rate, total growth rate, and RHEED intensity behavior of the specular beam, at the first out-of-phase condition, for slow (curves *a*) and fast (curves *b*) reaction rate (R_1) at single Ga sites. The former represents the reaction-limited–incorporation (RLI) growth mechanism whereas the latter, the configuration-limited, reactive- incorporation (CLRI) growth mechanism.

Ga migration kinetics inhibits subsequently arriving Ga atoms from providing the sites for attachment of As on the next layer. Towards the completion of the given Ga layer this is no longer the case and consequently As incorporation rate picks up, only to repeat the process. In such a case, since the group-V reaction rates are not the rate-limiting step in the growth, but the unavailability of the group-III atoms in an exposed state at the growth front does slow down the arsenic incorporation, it may be appropriate to refer to the growth mechanism as configuration-limited, reactive-incorporation (CLRI) growth. In either case, a predominantly layer-by-layer mode of material addition is achieved, and the growth process may generically be called a configuration-dependent, reactive-incorporation (CDRI) growth process.

The consequences of the CDRI growth process for the morphology of the nonequilibrium (i.e., growing) surface are many and varied, depending upon the competition among the molecular reaction rates and the Ga surface migration kinetics, on the fundamental time scale set by the chosen Ga flux at a given arsenic overpressure. For the kinetic rates employed in the obtaining of the results of Fig. 1, no significant formation and breakup of clusters is found during growth. For other combinations of the various kinetic rates, the CDRI model can and does produce[10] a growth process involving diffusion-controlled significant formation and breakup of Ga clusters with the Ga atoms either remaining on the surface or leaving for the vapor, depending upon the effective evaporation rate. In either case the diffusion-limited formation of two-dimensional critical Ga nuclei becomes a necessary requirement for As incorporation to occur at low As_2 reaction rates and/or pressure. Consequently, in either of these two cases, the growth process may be called the historical 2D nucleation mechanism of growth initiation if the notion is extended to include the need for critical nuclei of Ga atoms as being sufficient rather than the formation of critical nuclei of GaAs—the solid phase whose growth is under consideration. A direct test of which regime of the CDRI growth process—the two reaction-kinetics–controlled regimes explicitly discussed in this paper, or the diffusion-controlled 2D nucleation regime—is applicable under what growth conditions must await results of experiments which can unambiguously probe the dynamics of initial stages of cluster formation and breakup and the time-dependent growth rate.

GROWTH FRONT PROFILE

The CDRI model has demonstrated that under the usual MBE growth conditions where the incorporation rate of the group-III atoms is essentially unity, the single most important quantity controlling the smoothness of the growth front is the *effective* surface migration length (l_{eff}) of the group-III atoms on a time scale of order of its average arrival time interval (i.e., F_{III}^{-1}, where F_{III} is the flux), in relation to the average terrace width (W) of the starting substrate surface. When $W \gg l_{eff}$, a layer-by-layer mode of material addition occurs via a group-III local configuration-dependent reactive-incorporation process for the group-V molecular species and gives rise to the damped oscillatory nature of the observed RHEED intensity. For $W \ll l_{eff}$, the arriving group-III atoms are predominantly able to migrate to the existing steps and as a consequence, growth proceeds via step propagation from the very initiation and the relative distribution of the surface step density does not change with time. No oscillations in the RHEED intensity are then to be found. Indeed, the damped oscillatory nature of the oscillations, when seen, is a manifestation of (a) a starting surface for which $W > l_{eff}$ at growth initiation, and (b) the approach of (W) at the growth front towards the condition $\langle W \rangle < l_{eff}$ as the steady-state growth is reached, whence the oscillations are no longer observed. Thus, within the CDRI model the steady-state and static surface behavior can both be examined and understood within the same underlying atomistic kinetic processes by simply recognizing that for static surfaces the arrival time interval of group-III atoms is infinite so that the l_{eff} is such that atoms are always at step edges.

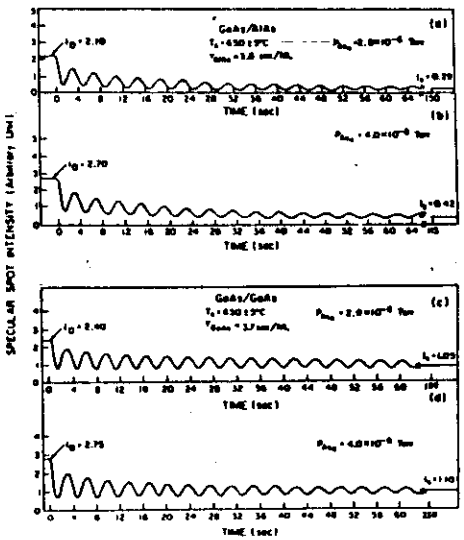

FIG. 3. Behavior of the specular beam intensity in the twofold direction during AlAs and GaAs growth on GaAs under an As-stabilized (2×4) RHEED pattern. The substrate temperature is 650 °C and the growth rate is

The resulting surface structural behavior of a binary compound, and the chemical distribution as well for a III–III–V alloy, has been shown to be significantly dependent upon the chosen T_s, P_V, τ_{III} and alloy composition through the dependence of l_{eff} on the interplay of various atomistic kinetic rates which themselves depend upon these user controlled parameters [3–7]. The effective migration length of the group III species may be viewed as taking the form [4,7],

$$l_{eff}^{\alpha} = \left\langle \left(h_i^{\alpha}(T_s, P_V)\ \tau_{ic}^{\alpha} \right)^{1/2} \right\rangle,$$

in which $h_i^{\alpha}(T_s, P_V)$ are the jump rates, at the chosen T_s and P_V, for the αth type of group III atom bonded in different local chemical and structural configurations denoted by i, and τ_{ic}^{α} is the lifetime of such a state which, depending upon the growth conditions, may be either the reaction time of group V molecule with the αth type of group III atom in the ith configuration or a time of the order of the arrival time of group III atoms from the vapour (i.e. inversely related to group III flux). For III–III–V alloys such as $Al_xGa_{1-x}As$, the relative migration and group V molecular reaction and desorption kinetics of the two group III atoms can lead to intrinsic asymmetry in the structural and chemical nature of the interfaces formed upon deposition of AlGaAs on GaAs (normal interface) and of GaAs on AlGaAs (inverted interface) [6,7]. A variety of variations on the usual practices of MBE growth may, in principle, be employed to reduce this undesirable consequence of the inherent difference in surface kinetics. Interruption of growth [8,16], usage of two different group V pressures each optimized for one type of material [10,13], pulsed heating, etc. are a few such alternatives. Of these, the first is now being increasingly explored [14,15,17–19] since our initial studies [8,16]. The CDRI model based computer simulations thus provide the needed connection between the surface kinetic processes and the resulting nature of the surface. This is illustrated in fig. 1 which shows the dynamics of the Ga effective migration length (panel a), the average terrace width, $\langle W_i \rangle$ (panel b), and the mean square fluctuation in the layer height, σ_h^2 (curve c), as a function of time during GaAs(100) homoepitaxy at the particular chosen growth conditions. Curve (d) of fig. 1 shows a parameter $S = \langle W_i \rangle \langle W_j \rangle / \sigma_h^2$ defined to represent an overall measure of the structural smoothness of the growth front. Finally, curve (e) shows the behavior of the RHEED specular beam intensity calculated, within a kinematical theory, at the first out-of-phase condition, $qd = \pi$, where d is the distance between

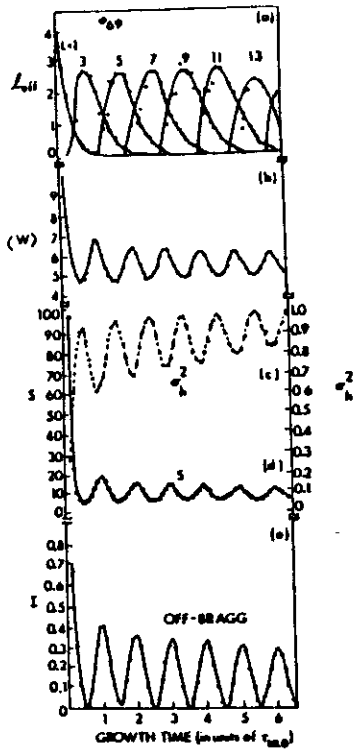

adjacent As or adjacent Ga(100) planes and q the electron momentum transfer normal to the surface. Note that oscillations in the RHEED intensity follow the behavior of the average terrace width and the smoothness parameter, thus indicating a correlation between the dynamics of the structural nature of the growth front and the behavior of the RHEED intensity.

Fig. 1. Results of the CDRI model based computer simulations of GaAs(100) homoepitaxy. Curve (a) the Ga effective migration length (l_{eff}) in each layer during the course of growth. Curve (b) the average terrace width, $\langle W_1 \rangle$, at the growth front, along the direction of the dangling bond orbitals. Curve (c) mean square fluctuation in the growth front profile. Curve (d) the smoothness parameter S (see text). Curve (e) the RHEED specular beam intensity at the first out-of-phase diffraction condition (see text). Note the connection between the RHEED intensity dynamics and the dynamics of the surface structural features.

Note the initial rapid drop of the average terrace widths caused by incorporation of Ga upon commencement of growth, followed by a damped oscillatory behavior. The maxima and minima are nearly coincident with the time of integral and half-integral Ga monolayer delivery (τ_{MLD}), respectively. Given that for the growth conditions chosen the Ga sticking coefficient is unity, τ_{MLD} is equivalent to the time of growth of a monolayer as well. The damping of the maxima in the average terrace width (measured in units of the surface nearest neighbor distance) is an indication of the roughening of the growth front profile with continued growth.

In Fig. 3 we present the temporal behavior of the specular beam intensity at three different growth temperatures for three different growth rates each, at the same As_4 pressure. the upper two panels of Fig. 3, when the substrate temperatures are near that corresponding to the I_{beam+}, the average intensity remains almost constant throughout the growth, implying that the average surface step distribution stabilizes quite rapidly under such conditions because of the favored surface migration near congruent temperature. At lower substrate temperatures the average intensity keeps decreasing slowly, even though it starts at a higher value because of the higher static state intensity. This indicates that although the growth is initiated on a smoother (i.e., the static) surface, the substrate temperature is not high enough to sufficiently stimulate the surface migration and consequently the growth front profile is degraded progressively. This degradation occurs faster with decreasing substrate temperature.[34]

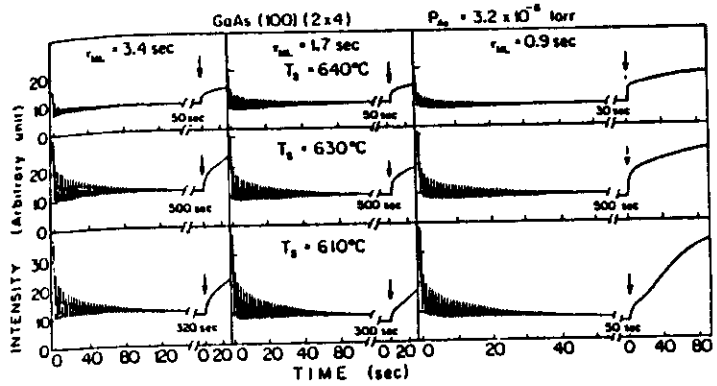

FIG. 3. The real-time RHEED specular beam intensity variations during GaAs(100) (2×4) growth at different growth rates and substrate temperatures but fixed P_{As_4} = 3.2 × 10^{-6} Torr. T_s = 630 °C is the substrate temperature corresponding to I_{beam+}. The arrows indicate the instant of growth termination. The dashed lines represent the average intensities.

Molecular Reactions at Steps:

While the explicit inclusion of the As_2^* incorporation rates in the computer simulations carried out by GM brought out the true essence of their proposed CDRI growth process, the Ga configurations considered were limited to the R_1, R_2, R_3 and R_4 intra-planar configurations shown in fig. It is, of course, entirely likely that As_2^* incorporation occurs at configurations involving Ga atoms in different atomic planes (i.e. at steps) with varying degree of significance. Thomsen and Madhukar (TM) have thus investigated[30] the role of reactions at the steps in order to ascertain its significance. They have also included several intraplanar Ga configurations involving 2 and 3 Ga atoms but arranged in all possible geometric configurations

In fig. (V.28), curve (a), we show the RHEED specular beam dynamics obtained[30] by TM for comparable, but low, As_2^* incorporation rates at the intraplanar and step configurations. Curve (b) corresponds to ignoring the step configurations and thus provides a reference for estimating their quantitative significance. Note the significantly faster damping of the RHEED oscillations in curve (a), even though only about 10% of the As_2^* incorporation occurred at the steps in these simulations.[30] Thus although the As_2^* incorporation events may be small in numbers, they can play a significant role in controlling the surface smoothness by adversely influencing the very inter-layer Ga migration process responsible for achieving a smooth growth front profile.

Finally, in fig. (V.30) curves (a) and (b) are shown the RHEED specular beam behavior found[30] by TM when all the As_2^* incorporation rates are increased ten-fold compared to fig. (V.28). This is equivalent to an increase in the As_4 pressure, as discussed before. Curve (b) corresponds to neglecting the step configurations. Hardly any difference is discernable between curves (a) and (b), thus confirming the CDRI model based expectation that at high As_4 pressure the significance of As_2^* reactions at steps is reduced since hardly any Ga atoms uncovered by As occur at the steps

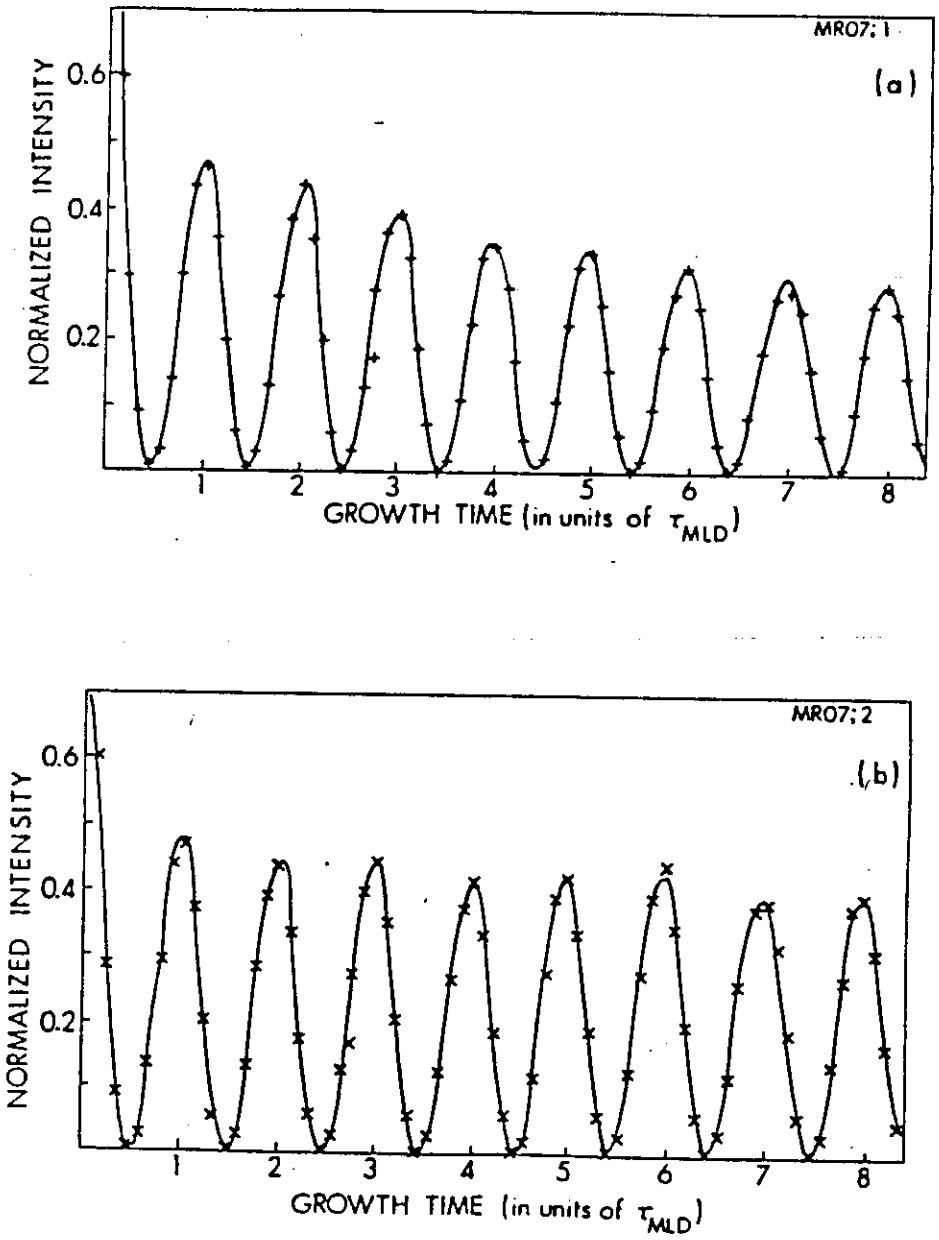

Fig. V 28

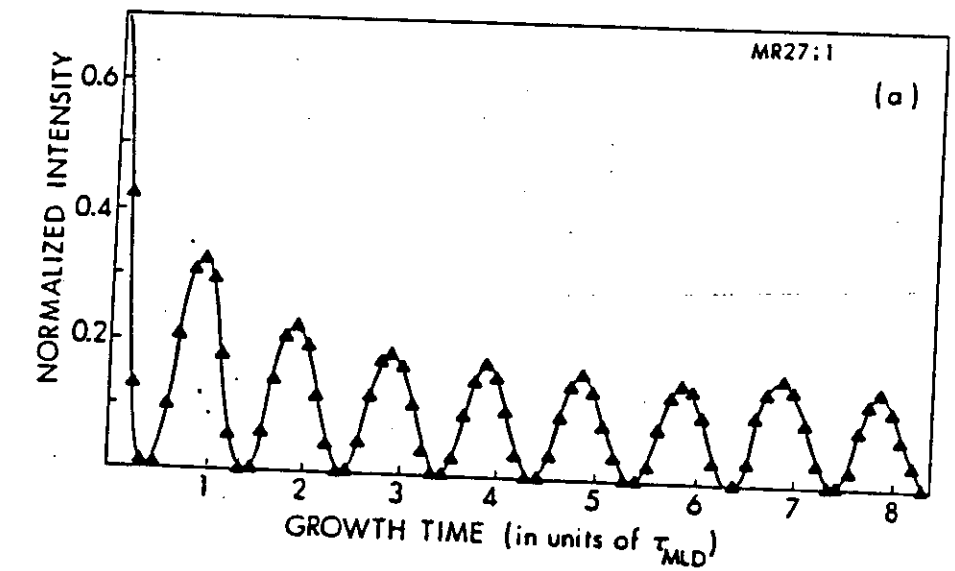

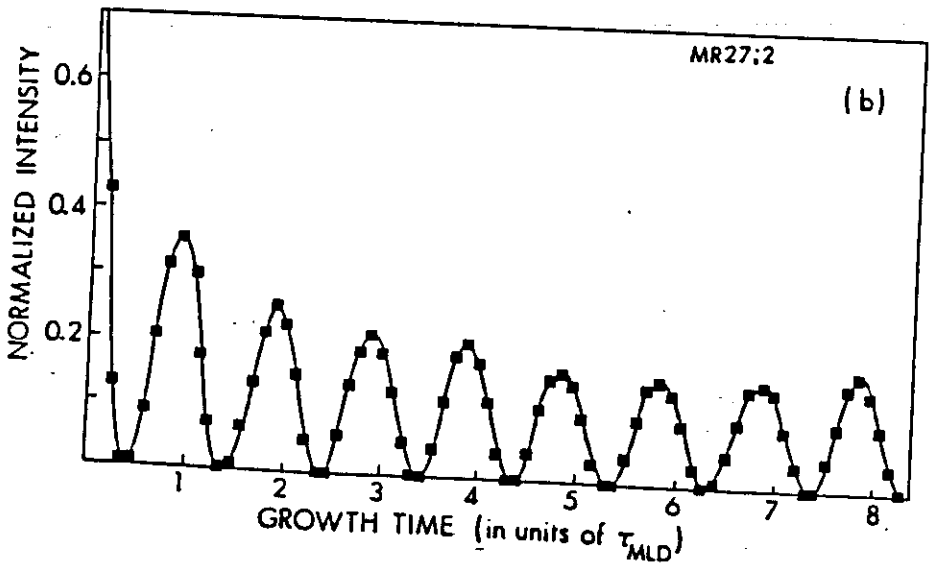

Fig. IV 30

CHAPTER IV

HETEROEPITAXIAL GROWTH

INTRODUCTION

one other important feature involved in the growth of a material A on a perfect substrate of a material B (i.e. heteroepitaxy) needs to be accounted for. Almost invariably the lattice constant of A is different from that of B, even when their crystal structures may be the same. The lattice mismatch, $(\Delta a/a)=((a_A-a_B)/a_A)$, induced strain is most certainly going to play a significant role in controlling the atomistic kinetic processes of surface migration and evaporation whose collective interplay will determine both the dependence of the nature of the growth mechanism as well as the nature of the surface morphology on the chosen growth conditions.

A thermodynamic description of the ground state of a single atomic overlayer on a substrate with a starting lattice mismatch $(\Delta a/a) = (a_l-a_s)/a_s$ was, however, provided[58] by Frank and Van der Merwe. Taking, as a model, the substrate and the overlayer to be elemental simple cubic structures, these authors showed that the total strain, $\epsilon_T=(\Delta a/a)$, can be accommodated homogenously in the overlayer up to a maximum value which was estimated to be nearly 15%. Beyond this maximum strain, only a part of the total strain, ϵ_H, can be accommodated homogenously and the remaining strain, ϵ_{MD} is accommodated in a localized fashion through generation of misfit dislocations. Thus,

$$\epsilon_T=\epsilon_H+\epsilon_{MD} \qquad \text{(II.12)}$$

and a positive value of ϵ_T implies compression in the overlayer with the extra atomic planes of the misfit dislocations lying in the substrate (i.e. a negative Taylor dislocation[57]). Correspondingly, a negative value of ϵ_T implies tensile strain in the overlayer and the

extra atomic "planes" defining the misfit dislocations lie in the overlayer (i.e. positive Taylor dislocations).

These considerations have been generalized[57] to overlayers of thickness greater than a monolayer, as well as to systems involving alternately deposited A and B materials in a multilayered structure, often referred to as a superlattice. As might be expected, for a single overlayer a lattice misfit $(\Delta a/a)$ dependent limiting thickness, d_c, is found below which the total strain can be accommodated homogeneously, but beyond which misfit dislocations will be generated to accommodate a part of the strain. In a superlattice involving the substrate material as one of the alternating materials, the same is true for the layers of both materials although the determination of the individual critical thicknesses becomes more involved due to internal compensating relaxation of strains.[57]. The situation in which the two (or more) alternating materials are different from the substrate is even more complicated.[57]

Some of the most prominent predictions are:
(i) mismatching at the interface is accommodated by misfit dislocations;
(ii) when the misfit and the thickness of the overgrowth are small enough the overgrowth is coherent, i.e. the misfit is entirely accommodated by a homogeneous strain in the film;
(iii) when the misfit and/or thickness is large enough both homogeneous strain and misfit dislocations are present;
(iv) a film whose growth is initially coherent becomes unstable at a critical thickness t_c and misfit dislocations are introduced at the free edges of the film; and
(v) as the film increases in thickness beyond t_c the homogeneous strain decreases.

CONTINUUM MODEL

This section reviews the stability of growing epitaxial films, predicted on the supposition that the stable configurations are those for which the energy is a minimum, i.e. eq. (2.12), namely

$$E = \text{minimum} \tag{6.1}$$

is valid.

MONOLAYERS[18-28])

The condition that an island overgrowth with rectangular boundaries at $x = \pm \frac{1}{2}L_x$ and $y = \pm \frac{1}{2}L_y$ be in equilibrium (stable or metastable) in the absence of external forces is that

$$\begin{aligned} T_x &= 0 \quad \text{at } x = \pm \tfrac{1}{2}L_x, \\ T_y &= 0 \quad \text{at } y = \pm \tfrac{1}{2}L_y, \end{aligned} \tag{6.2}$$

where T are the tensions

For a monolayer with a fixed number of atoms the condition (6.1) will be satisfied when the mean energy per atom $\bar{\varepsilon}$, is minimized, i.e. when

$$0 = \partial\bar{\varepsilon}/\partial\bar{e}_x = \partial\bar{\varepsilon}/\partial\bar{e}_y. \tag{6.5}$$

It accordingly follows that the condition for stable equilibrium is given by an equation of the form

$$1/P_x = 2E(k_x)/\pi k_x l_x + \sigma\bar{e}_y/\alpha_x \tag{6.7}$$

for the x-direction and an analogous one for the y-direction. Eq. (6.7) reduces to

$$1/P_2 = 2/\pi l(1 + \sigma) \tag{6.8}$$

to define the limiting misfit $1/P_2$ at which a coherent configuration, in the case of quadratic symmetry, becomes unstable.

Frank and van der Merwe[18]) have estimated – for a one-dimensional model – that the limiting misfits $1/P_1 = 2/\pi l$ and $1/P_1 = 1/l$, at which a coherent monolayer loses stability and metastability respectively, are approximately 9% and 14%. The limiting misfits $1/P_2$ for the two-dimensional model discussed above are related to $1/P_1$ by

$$1/P_2 = [(1 - \sigma)/(1 + \sigma)]^{\frac{1}{2}}(1/P_1). \tag{6.9}$$

The difference is seen to be due to the Poisson phenomenon and to infer a reduction of approximately 25% in the limiting misfits if σ is taken equal to $\frac{1}{3}$.

The dependence of relative mismatch $l/\bar{P}$ on relative misfit l/P at which the monolayer system is stable, is illustrated by curve A in fig. 8; curve B being predicted by the one-dimensional model. Along OC the mismatch $1/\bar{P}$ is zero showing that for misfits below those defined by eq. (6.8) the coherent configuration is stable and the misfit is entirely accommodated by homogeneous strain. As the relative misfit increases beyond the point C, the relative mismatch increases very rapidly by a process in which misfit dislocations are fed into the interface at the free edges. Theoretically, the misfit will always be partially accommodated by homogeneous strain as is manifested by the fact that $1/\bar{P}$ is always less than $1/P$.

An important result of the one-dimensional calculations, apart from the difference in the limiting misfits defined by points C and D is that in this model the limiting misfit is critical by having a vertical slope at D, predicting

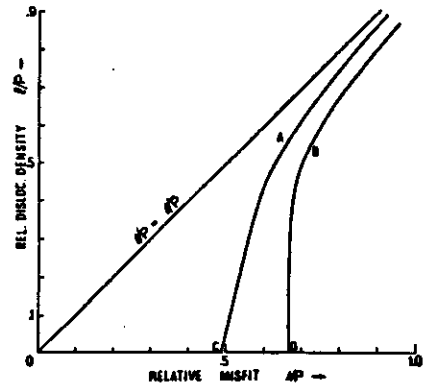

Fig. 8. Graph of relative mismatch $l/\bar{P}$ versus relative misfit l/P for which monolayer is stable; OC and curve A being for relation (6.7) and OD and curve B for the Frank and van der Merwe model.

THICKENING OVERGROWTHS

The total energy E_t of a system comprising an epitaxial overgrowth of finite thickness t on a thick (semi-infinite) substrate may be written in the form[18])

$$E_t = E_{\text{II}}S_0 + (E_d^x + E_d^y)S + E_f + E_{sd}, \tag{6.11}$$

where S_0 is the interfacial area when the film strain $\bar{e}$ vanishes, S the area when $\bar{e}$ is not zero, E_{II} the energy of homogeneous strain per unit interfacial area when $\bar{e} \neq 0$, E_d^i the average misfit dislocation energy per unit interfacial area for misfit in the i-direction ($i = x, y$) under the existing strain $\bar{e}$, E_f the total free energy of the free surface of the overgrowth and E_{sd} the total adhesive energy for the coherent configuration. E_{sd} is, by definition, independent of strain. E_f is supposed to be independent of strain, thereby ignoring the strain dependence predicted by Drechsler and Nicholas[21]). The minimization of E_t is therefore equivalent to the minimization of

$$E_T S_0 = E_{\text{II}}S_0 + (E_d^x + E_d^y)S,$$

or

$$E_T = E_{\text{II}}(\bar{e}) + 2E_d(\bar{e})(1 + \bar{e})^2, \tag{6.12}$$

The energy E_T is minimized for a strain $\bar{e}_m$ defined by

$$\partial E_T/\partial\bar{e} = 0, \qquad \bar{e} = \bar{e}_m. \tag{6.15}$$

Ball[18]) has calculated the relation between $\bar{e}_m$ and t for the case of Cu on Ag using the expression for E_d in the equilibrium equation (6.12). The corresponding misfit of -13% is so large that a coherent overgrowth is unstable, even for a monolayer.

Curve A (fig. 9), for Ball's model, and curve B, for the simple model, have been constructed

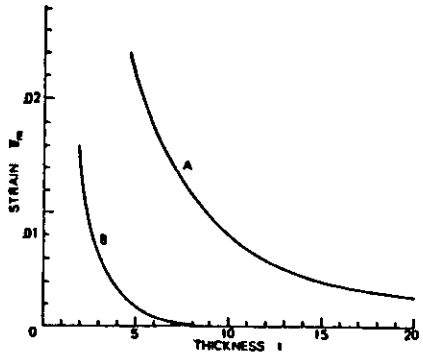

Fig. 9. Dependence of equilibrium strain ℓ_m on overgrowth thickness t in eq. (6.20) (units of a) for Cu on Ag. Curve A: model of Ball, curve B: Simple model of Frank and van der Merwe.

The dependence of the limiting thickness t_c on coherent strain e_0, has also been calculated by Ball [18] from his model. The result is illustrated in fig. 10 for an average case in which $\mu_a = \mu_b = \mu_0$ and $\sigma = 0.3$.

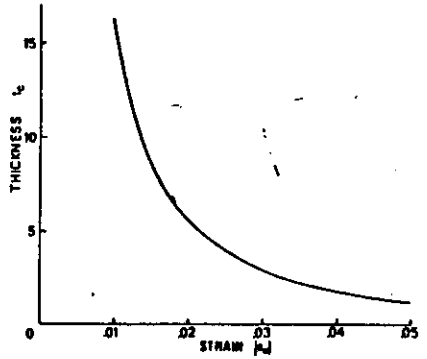

Fig. 10. Dependence of limiting thickness t_c (at which coherent overgrowth becomes unstable) on the magnitude $|e_0|$ of the coherent strain (see eq. (6.24)).

2. Potential energy functions with a many-body contribution

The Born–Oppenheimer approximation [4] provides an unambiguous definition of a potential energy function for the nuclei which depends only upon their positions and implicitly contains the energy of the ground state electronic wavefunction that binds them together. If there are no external fields acting on the system, then this potential depends only on the relative positions of the nuclei, which we will refer to hereafter as the atomic positions, and can be expanded quite generally in a manybody series [5]:

$$\Phi(x_1,\ldots,x_N) = \frac{1}{2!}\sum_{i\neq j}\sum V^{(2)}(r_{ij}) + \frac{1}{3!}\sum_{i\neq j\neq k}\sum\sum V^{(3)}(r_{ij},r_{ik},r_{jk}) + \ldots + \frac{1}{n!}\sum_{i\neq\ldots\neq n}\cdots\sum V^{(n)}(r_{ij},\ldots,r_{kl},\ldots). \quad (1)$$

The n-body potentials $V^{(n)}(\ldots)$ are functions of the positions of n atoms taken at a time, and are evaluated for all distinct n-tuples of atoms.

To put eq. (1) to practical use, one chooses a basic functional form for each $V^{(n)}$ which contains a few adjustable parameters. The parameters are then selected to give the best representation of the atomic interactions by fitting the calculated energies and structures to available experimental data. When two or more types of atoms interact, different $V^{(n)}$ are needed for each distinct combination of atom types. This is usually handled by selecting different values for the parameters from the same basic potential function. The resulting PEF's are semi-empirical approximations to the exact Born–Oppenheimer potential.

Two-body contributions alone are categorically unable to properly describe molecular configurations for molecular clusters in the gas phase, so why should one think that such potentials can properly describe clusters on a surface. Based on *any* two-body potentials alone, a trimer in the gas phase will always be a planar equilateral triangle while a tetramer will always be a cluster of tetragonal packing. However, in nature, many trimers and tetramers are linear molecules. For example, Si_3, C_3, C_4, SiC_2, etc. are linear molecules. It is only when one includes the many-body effect that one can predict the linear molecule to be more stable than the equilateral triangle molecule for the trimer. If one uses a three-body potential of the Axilrod–Teller type [1] to model the many-body effect, then only a single additional parameter, Z (see eq. (2b)), is needed to describe the potential energy function (PEF). In fig. 1a, a plot of the intermolecular potential as a function of the reduced parameter Z^* (see eq. (3b)) is given for a number of different cluster shapes [5]. We note that large values of Z^* favor the linear cluster morphology. From such calculations with a PEF involving both two-body and three-body terms,

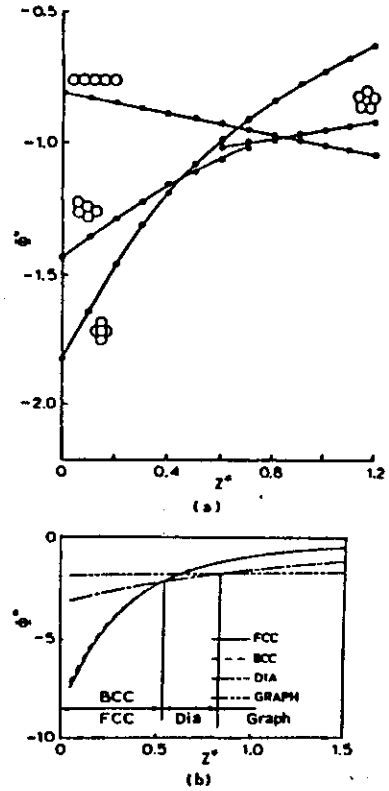

Fig. 1. (a) Schematic plot of reduced PEF, Φ^*, as a function of the reduced three-body parameter, Z^*, for several cluster shapes. (b) Φ^* versus Z^* for several different crystallographic structures.

the two-body term favors close-packed structures while the three-body term favors open structures so that the combination of the two provides a balance [1]. In fig. 1b, we see the dependence of bulk crystallographic structural stability on Z^*.

As a second example to illustrate the importance of the many-body effect on surface considerations, consider the surface region atomic interlayer spacings which are experimentally found to differ considerably from the bulk. In general, the most pronounced relaxation occurs in the spacing between the first and second atomic layers, d_{12}, which is found to be less than the bulk value. However, theoretical predictions, using only semi-empirical pair potentials, always predict d_{12} to be larger than the bulk value. Because of their functional simplicity, such pair-potential-only models prohibit their usage for modeling surface region effects in a truly meaningful fashion.

In this work, we use the following n-body potential functions:

$$V^{(2)}(r_{ij}) = \frac{\varepsilon}{m-n}\left[n\left(\frac{R_0}{r_{ij}}\right)^m - m\left(\frac{R_0}{r_{ij}}\right)^n\right], \quad (2a)$$

$$V^{(3)}(\ldots) = Z\left[\frac{1+3\cos\theta_{ij}\cos\theta_{ik}\cos\theta_{jk}}{(r_{ij}r_{ik}r_{jk})^3}\right], \quad (2b)$$

$$V_{(n)}(\ldots) = 0 \quad (\text{for all } n>3). \quad (2c)$$

Eq. (2a) is the two-body Mie (or generalized Lennard-Jones) potential [6] and eq. (2b) is the three-body Axilrod–Teller potential [5,7].

There is no direct theoretical justification for using these potentials, and in particular the Axilrod–Teller potential, to model the short-range interactions in covalently bonded systems. The Axilrod–Teller function was chosen for the purely pragmatic reasons that it stabilizes linear clusters and favors open crystal structures [8]; a minimum requirement for simulating Si or C systems. The Axilrod–Teller potential also has a fairly simple analytic form which makes it computationally convenient.

There are several possible choices present today for a Si PEF involving the sum of two-body and three-body considerations [3–5] and they differ in the minimum number of parameters needed to define the PEF. These range from 3 [3] to 18 [5]. The problem is even more severe for the binary case like GaAs where the minimum number of defining parameters has expanded from 3 to 10. Extension to the ternary Ga–Al–As case such as considered in this paper requires the minimum number of defining parameters to increase to 22. Thus, although the effective two-body (Lennard-Jones) and three-body (Axilrod–Teller) contributions are slightly simplistic with respect to modeling the details of solid state interactions, there is insufficient experience and insufficient data available to handle a more complex and more realistic potential when one wants to apply it to a ternary system like Ga–Al–As.

The parameter set given in table 1 was generated for the Ga–Al–As system. The total interaction energy in the repeat cell is given by

$$\Phi = \sum_{\alpha=1}^{2}\sum_{\beta=1}^{2}\varepsilon_{\alpha\beta}\left[\left(\frac{r_{0(\alpha\beta)}}{d}\right)^{12}A_{\alpha\beta} - 2\left(\frac{r_{0(\alpha\beta)}}{d}\right)^{6}B_{\alpha\beta}\right] + \sum_{\alpha=1}^{2}\sum_{\beta=1}^{2}\sum_{\gamma=1}^{2}\frac{Z_{\alpha\beta\gamma}}{d^9}T_{\alpha\beta\gamma}, \quad (1a)$$

where α, β and γ indicate the type of atoms (Ga, Al or As), d is the equilibrium nearest neighbor distance, $\varepsilon_{\alpha\beta}$ and $r_{0(\alpha\beta)}$ are the Lennard-Jones parameters while $Z_{\alpha\beta\gamma}$ is the Axilrod–Teller parameter and

$$A_{\alpha\beta} = \frac{1}{2!}\sum_{i}^{N_\alpha}\sum_{j}^{N_\beta}\left(\frac{d}{r_{ij(\alpha\beta)}}\right)^{12},$$

$$B_{\alpha\beta} = \frac{1}{2!}\sum_{i}^{N_\alpha}\sum_{j}^{N_\beta}\left(\frac{d}{r_{ij(\alpha\beta)}}\right)^{6}, \quad (1b)$$

$$T_{\alpha\beta\gamma} = \frac{1}{3!}\sum_{i}^{N_\alpha}\sum_{j}^{N_\beta}\sum_{k}^{N_\gamma}\left[1+3\cos\theta_i\cos\theta_j\cos\theta_k \times\left(\frac{r_{ij(\alpha\beta)}}{d}\frac{r_{jk(\beta\gamma)}}{d}\frac{r_{ki(\gamma\alpha)}}{d}\right)^{-3}\right]. \quad (1c)$$

In eqs. (1), θ_i, θ_j, θ_k and r_{ij}, r_{jk}, r_{ki} represent the angles and sides of the triangle formed by only three atoms i, j and k while $A_{\alpha\beta}$, $B_{\alpha\beta}$ and $T_{\alpha\beta\gamma}$ are lattice sums depending only on the crystal structure and not the atomic properties of the atoms [6].

Using this PEF and the parameters listed in table 1, an excellent fit was found to the zinc-blende structure, the lattice parameter change between GaAs and AlAs for $Ga_xAl_{1-x}As$ alloys, the GaAs specific heat, the GaAs(110) reconstruction pattern, the (2 × 2) GaAs(111) reconstruction pattern as well as the various cohesive energies indicated in fig 1. The PEF does not reproduce the bulk modulus well. This would require another term in the three-body contribution which would then grow by 10 additional parameters for the ternary system.

Table 1
Potential energy parameters for Ga–Al–As system

Two-body parameters [a]			Three-body intensity parameters	
	$\varepsilon_{\alpha\beta}$ (eV)	$r_{0(\alpha\beta)}$ (Å)		$Z_{\alpha\beta\gamma}$ (eV Å^9)
Ga–Ga	1.004	2.461	Ga–Ga–Ga	1826.4
As–As	1.164	2.491	As–As–As	2151.9
Al–Al	1.216	2.520	Al–Al–Al	2241.0
Ga–As	1.738	2.448	Ga–Ga–As	1900.0
Ga–Al	1.121	2.490	Ga–As–As	4600.0
Al–As	2.06	2.43	Ga–Ga–Al	1955.3
			Ga–Al–Al	2093.3
			Al–Al–As	3000.0
			Al–As–As	5000.0
			Ga–Al–As	2500.0

[a] Power of repulsive arm, $m = 12$; power of attractive arm, $n = 6$

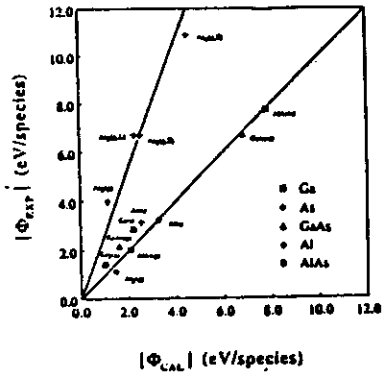

Fig. 1. Comparison of experimental with calculated cohesive energies for a variety of molecular species in the solid and gas phases using the present semiempirical PEF.

The pair-correlation function $g(r)$ offers a convenient way to observe and analyze local order in condensed systems.[9,7] This function is defined to be proportional to the mean number of atom pairs with vector separation r, averaged over all directions of r, with normalization to unity for a random distribution of atoms.

Figures 4 and 5, respectively, show $g(r)$ extracted from crystal- and liquid-phase molecular-dynamics runs near T_m^*. The first of these is highly structured, revealing the organization of atoms into well-defined coordination shells.

$$T^* \equiv k_B T/\varepsilon .$$

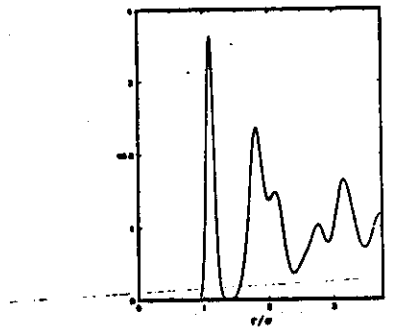

FIG. 4. Pair-correlation function for the Si model in the crystal phase at $T^* = 0.0800$.

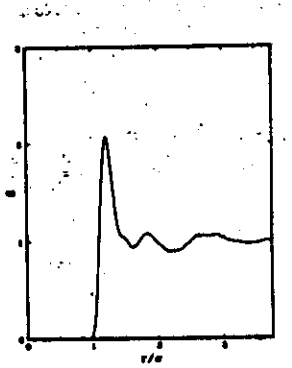

FIG. 5. Pair-correlation function for the Si model in the liquid phase at $T^* = 0.0817$.

the ledge excess energies as a function of ledge spacing d_y are plotted in fig. 5. In fig. 5, the legend ledge 1/ledge 2 next to each curve means that the ledge 1 energy is being determined while the spacing to ledge 2 is changing.

The negative excess energy for the upper $[2\bar{1}\bar{1}]$ ledge at large ledge spacings implies a beneficial face reconstruction in the vicinity of the ledge compared to that found for the flat (111) surface without ledges. Spontaneous formation of such ledges cannot occur without concurrent formation of adjacent ledges to complete the cluster and this could make the net energy change positive. How-

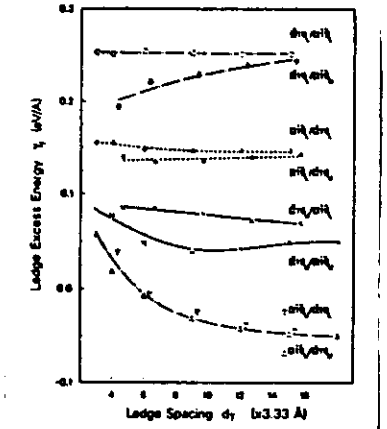

Fig. 5. Ledge energies, γ_y versus ledge spacing, d_y, for a variety of ledge pairs. The legend Ledge 1/Ledge 2 corresponds to ledge 1 energy as the spacing to ledge 2 is changed.

MOLECULAR MECHANICS

The expression "molecular mechanics" is currently used to define a widely used calculational method designed to give accurate a priori structures and energies for molecules. The method is a natural outgrowth from older ideas of bonds between atoms in molecules, and van der Waals forces between nonbonded atoms. It employs the fundamental formulations of vibrational spectroscopy, and some of the basic ideas behind this procedure can be traced back to D. H. Andrews (1930) (*1*). The basic idea is that bonds have "natural" lengths and angles, and molecules will adjust their geometries so as to take up these values in simple cases. In addition, steric interactions are included using van der Waals potential functions. In more strained systems, the molecules will deform in predictable ways with "strain" energies that can be accurately calculated.

Molecular mechanics calculations employ an empirically derived set of equations for the Born–Oppenheimer surface whose mathematical form is familiar from classical mechanics (*9–20*). This set of potential functions, called the force field, contains adjustable parameters that are optimized to obtain the best fit of calculated and experimental properties of the molecules, such as geometries, conformational energies, heats of formation, or other properties.

To understand molecular mechanics force fields, it is convenient to start with the formalism of force fields appropriate for vibrational analysis.

When a molecule with n atoms, defined in terms of $3n$ coordinates, x_i, is deformed from its geometry of minimum potential energy, V_0, and coordinates, x_0, the potential energy may be written in a Taylor series expansion as:

$$V_{pot} = V_0 + \sum_{i=1}^{3n} \left(\frac{\partial V}{\partial x_i}\right)_0 \Delta x_i + \frac{1}{2} \sum_{i,j=1}^{3n} \left(\frac{\partial^2 V}{\partial x_i \partial x_j}\right)_0 \Delta x_i \Delta x_j + \frac{1}{6} \sum_{i,j,k=1}^{3n} \left(\frac{\partial^3 V}{\partial x_i \partial x_j \partial x_k}\right)_0 \Delta x_i \Delta x_j \Delta x_k + \text{higher terms} \quad (2.1)$$

In the vibrational analysis of a molecule having a geometry corresponding to an energy minimum, the first term, V_0, is taken as zero.[1] From the definition of a potential minimum it follows that at this geometry the first derivative term also vanishes. For sufficiently small displacements, as ordinarily treated in vibrational analysis, the terms higher than quadratic are neglected (harmonic approximation) (*1–4*). The potential energy depends only on the third term, to a first approximation, and if we replace the second derivatives, which are called the force constants, by their symbols f_{ij}, we are left with the simple relationship of a harmonic force field,

THE most useful phenomenological description of the short-range valence forces in the tetrahedrally coordinated crystals is the valence-force-field (VFF) approach,[1] in which all interatomic forces are resolved into bond-stretching and bond-bending forces.

The VFF model for diamond-structure crystals has been described by Musgrave and Pople.[1] For the purpose of this paper we simplify their expressions omitting the less important forces. The simplified expression for the VFF part of the distortion energy of each unit cell is

$$U=\tfrac{1}{2}\sum_{s=1}^{2}\sum_{i=1}^{4}k_r(\Delta r_i)^2+\sum_{s=1}^{2}\Big[\tfrac{1}{2}\sum_{i,j>i}k_\theta{}^s(r\Delta\theta_{ij}{}^s)^2 + \sum_{i,j\neq i}k_{rr'}{}^s(\Delta r_i{}^s)(r\Delta\theta_{ij}{}^s)+\sum_{i,j>i}k_{rr}{}^s(\Delta r_i{}^s)(\Delta r_j{}^s)\Big], \tag{1}$$

in the notation of Musgrave and Pople.[1] In (1) we have allowed the force constants $k_\theta{}^s$, etc., to differ for the two atoms in the unit cell denoted by $s=1, 2$. The bonds about each atom are denoted by $i, j=1, \ldots, 4$, r is the equilibrium bond length, $\Delta r_i{}^s$ is the scalar change in length of bond i about atom s, and $\Delta\theta_{ij}{}^s$ is the change in angle formed by bonds i and j about s, as shown in Fig. 1. Only the bonds about one atom are included in the first term in (1) to avoid double counting in the sum over unit cells.

The formulas for the elastic constants can be further simplified by an approximation suggested by Keating.[4] Assume that the expansion of the VFF energy (1) involves only the squares of the scalar variations $\Delta(\mathbf{r}_i{}^s\cdot\mathbf{r}_j{}^s)$, where $\mathbf{r}_i{}^s$ and $\mathbf{r}_j{}^s$ are bond vectors about atom s. Then in Keating's notation, we have

$$U=\tfrac{1}{2}\alpha\Big(\frac{3}{4r^2}\Big)\sum_{s=1}^{2}\sum_{i=1}^{4}[\Delta(\mathbf{r}_i{}^s\cdot\mathbf{r}_i{}^s)]^2 + \tfrac{1}{2}\sum_{s=1}^{2}\beta^s\Big(\frac{3}{4r^2}\Big)\sum_{i,j>i}[\Delta(\mathbf{r}_i{}^s\cdot\mathbf{r}_j{}^s)]^2. \tag{9}$$

One may readily show by expressing (9) in terms of changes in bond lengths and angles that Keating's approximation is realized in the VFF model by requiring

$$k_r=3\alpha+\tfrac{1}{2}\beta, \quad k_\theta=\tfrac{1}{2}\beta, \quad k_{rr'}=(3\sqrt{2})^{-1}\beta, \quad k_{rr}=-\tfrac{1}{12}\beta, \tag{10}$$

where, as before, $\beta=\frac{1}{2}(\beta^1+\beta^2)$.

one may easily show that the elastic constants have the simple form

$$C_{11}+2C_{12}=(\sqrt{3}/4r)(3\alpha+\beta)-0.355SC_0, \tag{11a}$$

$$C_{11}-C_{12}=(\sqrt{3}/r)\beta+0.053SC_0, \tag{11b}$$

$$C_{44}=(\sqrt{3}/4r)(\alpha+\beta)-0.136SC_0 - C_1{}^2, \tag{11c}$$

where

$$C=(\sqrt{3}/4r)(\alpha+\beta)-0.266SC_0 \tag{11d}$$

and

$$\zeta=C^{-1}[(\sqrt{3}/4r)(\alpha-\beta)-0.294SC_0]. \tag{11e}$$

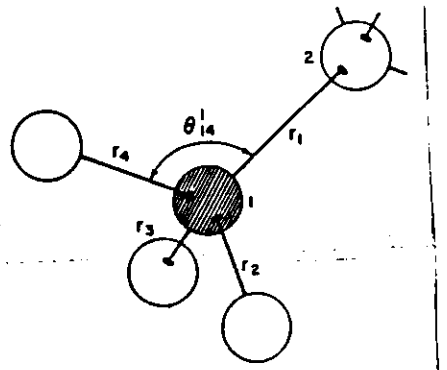

FIG. 1. Cubic ZnS (ZB or sphalerite) structure. The bonds shown are considered to belong to the unit cell containing atoms 1 and 2, and a typical angle θ_{14} is shown.

In Table I are listed the experimental elastic constants of the ZB crystals, the parameter $S=Z^{*2}/\epsilon$, and the constant C_0. From the experimental values the parameters for Keating's approximation are derived and shown in Table II.

TABLE I. Experimental bond lengths, elastic constants, and effective charge parameter S for the diamond or sphalerite structure materials. The elastic constants and effective charge parameters are for room temperature for each case in which that data was available.

Material	r (a.u.)	C_0	C_{11} (10^{11} dyn/cm^2)	C_{44}	C_{12}	S
C	2.919	40.523	107.6	57.68	12.50[a]	0
Si	5.444	7.538	16.57	7.96	6.39[b]	0
Ge	5.529	6.401	12.89	6.71	4.83[b]	0
AlSb	5.020	4.630	8.94	4.16	4.43[c]	0.364[d]
GaP	4.460	7.430	14.12	7.05	6.25[e]	0.514[f]
GaAs	4.626	6.418	11.81	5.92	5.32[e]	0.441[f]
GaSb	5.006	4.681	8.84	4.32	4.03[e]	0.331[f]
InP	4.802	5.529	10.22	4.60	5.76[f]	0.682[g]
InAs	4.939	4.941	8.33	3.96	4.53[e]	0.579[h]
InSb	5.301	3.723	6.67	3.02	3.65[e]	0.369[h]
ZnS	4.426	7.660	10.40	4.62	6.50[i]	0.887[g]
ZnSe	4.638	6.356	8.10	4.41	4.88[j]	0.688[k]
ZnTe	4.984	4.765	7.13	3.12	4.07[l]	0.539[k]
CdTe	5.303	3.718	5.35	1.99	3.68[e]	0.838[k]
CuCl	4.423	7.681	2.72	1.57	1.87[l]	0.266[m]

[a] M. J. Mehlman and W. L. Bond, Phys. Rev. 105, 116 (1957).
[b] M. B. Hunaerson, in *Solid State Physics*, edited by F. Seitz and D. Turnbull (Academic, New York, 1958), Vol. 7.
[c] *Landolt-Börnstein Numerical Data and Functional Relationships in Science and Technology, New Series*, edited by K. H. Hellwege (Springer, Berlin, 1966), Group 3, Band 2.
[d] A. Mooradian and G. B. Wright, Solid State Commun. 4, 431 (1966).
[e] R. Keyes and W. O. Groves, J. Appl. Phys. 39, 4049 (1968).
[f] A. J. Bergeret Phys. Rev. 185, 917 (1968).
[g] M. H. Mecklenburg, A. Javanovich, P. Andreatch, and T. B. Bateman, J. Appl. Phys. 39, 4117 (1968).
[h] D. H. Martin, Advan. Phys. 14, 39 (1965).
[i] F. L. Richardson and W. R. Grayson, J. Appl. Phys. 37, 462 (1966).
[j] Reference 16.
[k] R. C. Nelson, in *Light Scattering Spectra of Solids*, edited by G. B. Wright (Springer, New York, 1969), p. 129.
[l] Reference 15.
[m] A. Madan, F. Brehm, J. Chandel, and P. Sartorius, J. Chem. Phys. 49, 471 (1968).

TABLE II. Theoretical quantities derived from the data of Table I. α and β are the short-range force parameters and ζ is Kleinman's internal displacement parameter.

Material	α	β	β/α	Ratio[a]	ζ	Optic-mode check[b]
	α/m					
C	129.33	84.76	0.655	1.002	0.208	1.159
Si	48.50	13.81	0.285	1.005	0.557	1.044
Ge	38.67	11.35	0.294	1.081	0.546	1.019
AlSb	35.35	6.77	0.192	1.056	0.649	1.083
GaP	47.32	10.44	0.221	1.044	0.589	1.105
GaAs	41.19	8.95	0.217	1.068	0.600	1.085
GaSb	35.16	7.22	0.218	1.059	0.612	1.039
InP	43.04	6.24	0.145	1.075	0.699	1.136
InAs	35.18	5.50	0.156	1.109	0.682	1.054
InSb	29.61	4.77	0.161	1.103	0.695	1.029
ZnS	44.92	4.78	0.107	1.082	0.736	1.300
ZnSe	35.74	4.23	0.120	1.319	0.723	1.210
ZnTe	31.35	4.45	.142	1.059	0.706	1.250
CdTe	29.02	2.43	0.084	1.045	0.793	1.220
CuCl	12.60	1.00	0.079	1.552	0.785	0.978

[a] Left-hand side of Eq. (13).
[b] ω_t(model)/ω_t(expt.). See Eq. (16).

[1] W. Cady, *Piezoelectricity* (McGraw-Hill, New York, 1946).

Interaction Energies	Harmonic Approximation	Anharmonic term
Stretching Energy	$E_c = \frac{1}{2} k_c (l - l_0)^2$	$1 + c_c (l - l_0)$
Bending Energy	$E_\theta = \frac{1}{2} k_\theta (\theta - \theta_0)^2$	$1 + c_\theta (\theta - \theta_0)$
Van der Waals Energy	$E_{vdw} = k \exp(r/R) - k_{vdw}/R^6$	
Stretch-bend Energy	$E_{sb} = (k_{sc1} \Delta l_1 + k_{sc2} \Delta l_2) \Delta\theta$	
Torsion Energy	$E_t = + (V_1/2)(1 + \cos\omega)$	
Electrostatic Energy	$E_e = \frac{1}{2} \sum_{ij} q_i q_j / R_{ij}$	

Table 1

HETEROEPITAXIAL MODELS

The heteroepitaxial growth of CdTe on (100) oriented GaAs has been a subject of recent interest because of its potential applications in optoelectronic devices and especially in infrared imaging focal plane arrays.[1,2] High quality CdTe films have been grown epitaxially on GaAs (100) by vacuum evaporation,[3] molecular beams,[4–9] laser assisted deposition,[10] organometallic vapor phase,[11] hot wall vacuum evaporation,[12] and close-spaced vapor transport.[13] Although the current models are successful in describing some of the experimental observations,[9,10] two important points are not accounted for: How can epitaxy take place despite a very large lattice mismatch (14.6%) and why is the grown layer either (100) or (111) oriented[14–17] depending on the structure of the GaAs surface?

FIG. 1. Schematic of a tetrahedral unit cell formed on As-deficient (100)As surface of GaAs(a), and of a twin tetrahedral unit cell formed on Ga-stabilized (100)Ga surface of GaAs(b).

It has been found[5,16] that the epitaxial growth proceeds initially by the adsorption of about one monolayer of Te, which can change the resulting CdTe orientation.[10,16] The role of Te is taken into account in one model based on both chemical bonding and lattice matching considerations as suggested first by Otsuka *et al.*[16] A two-stage mechanism is proposed with stable monolayer islands formed before multilayer growth takes place. The basic unit cells forming the stable islands are of two kinds: a tetrahedral $\frac{Ga}{Ga}>$ Te–As cell as illustrated in Fig. 1(a) leading to (111) orientation growth and a twin tetrahedral $\frac{Ga}{Ga}>$ Te–Te–Te$<\frac{Ga}{Ga}$ structure giving rise to preferential (100) orientation [Fig. 1(b)]. The factor influencing the formation of either kind of cell is the composition of the GaAs surface: the tetrahedral unit cell is formed on the As-deficient surface whereas the twin tetrahedral structure develops on the As- or Ga-stabilized surface.

Concerning the (111) orientation growth, let us consider a (100) As surface of GaAs with around one half of the As atoms missing. Thus the real substrate appears as a double plane, separated by 1.41 Å, one plane having some Ga with one dangling bond (in the space freed by the missing As) located in the (0$\bar{1}$1) plane perpendicular to (011) where the two dangling bonds of the superficial remaining As atoms are.

Each Te atom impinging on this surface takes place in a selective site of the (011) plane binding with one As and two Ga-first neighbors in the lower plane through a small rotation of the dangling bonds, as seen in Fig. 1(a). This effect of relaxation could be interpreted in terms of surface rehybridizations.[19] This construction leaves one dangling bond, nearly perpendicular to the (100) surface, per each threefold bound Te atom.

Now Cd atoms can tie the Te dangling bond and initiate the multilayer growth process with (111) CdTe parallel to (100) GaAs in the [1$\bar{1}$1] direction. This mechanism implies, therefore, that the basic Te atoms have to move laterally on the initial surface leading to small distortions in the basic tetrahedral structures, in such a way that the repetition of the structure is limited along the [011] axis. A sequential two-two or two-three rows structure is expected, as schematized in Fig. 2. On the other hand, no limitation appears along the rows in the [0$\bar{1}$1] direction. It is to be noted that these sequences produce no defect in the lattice configuration of the (111)CdTe layer. Thus, the CdTe layer, which is obviously (1$\bar{1}$1) oriented, exhibits the epitaxial relations [$\bar{2}$11]$\parallel$[0$\bar{1}$1]GaAs and [0$\bar{1}$1]$\parallel$[011]GaAs. The interatomic planar spacing along the [$\bar{2}$11] direction is found to be 7.995 Å, matching to within 0.7% with the corresponding value for bulk CdTe (7.938 Å).

In a first approximation one can take for Ga–Te and As–Te the value of Cd–Te bond length $d = 2.806$ Å. One can show that the Te atom is located at a site slightly up (0.15 Å) the (100) As plane with trihedral angles GaTeGa = 90°8 and GaTeAs = 112°8, which are to be compared with 109°5

type of configuration exhibits a mirror symmetry with respect to the $(0\bar{1}1)$GaAs plane. Although the actual value for the bond length is probably smaller it will be seen later that the conclusions reached are not invalidated.

This model takes into account the conclusions reported for the (111) orientation[16,18,19] showing that the growth starts with "adsorption" of Te atoms. Indeed it is known that Te has a much higher sticking coefficient than Cd on GaAs.[20] This is also to be correlated with the results of molecular beam epitaxy (MBE) experiments based on setting up a GaAs-Te precursor surface to (111)CdTe growth.[3]

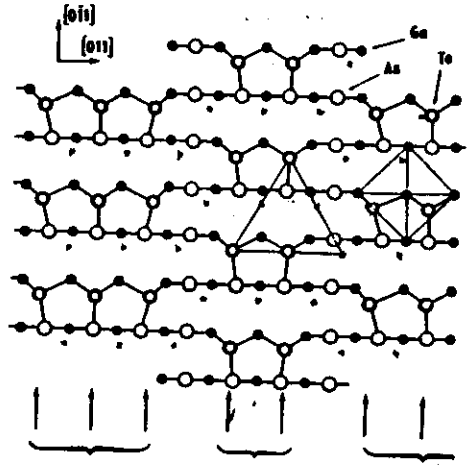

FIG. 2. Sequential structure—three-two rows—of tetrahedral unit cells formed on As-deficient (100)GaAs surface, leading to (111)CdTe growth.

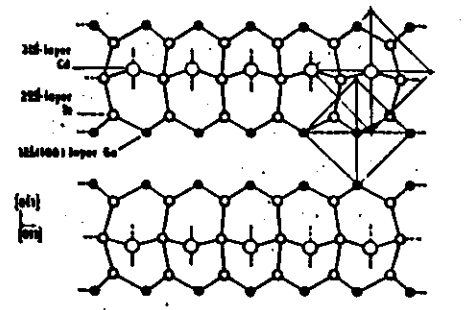

FIG. 4. Clusters formed on (100)Ga surface of GaAs, leading to (100)CdTe parallel growth. Only atoms involved in bonds are represented.

In order to understand the (100) growth let us consider now a Ga-stabilized (or As-stabilized) surface as obtained by means of chemical etches[18,22] and/or heat treatments prior to growth.[4,8,9,23] This surface presents two dangling bonds on each Ga atom. In a first step Te atoms take place in the position that would be occupied by the first missing As atoms, along the [011] axis, forming sp^3-like bonds with two Ga. In a second step two such base-bound Te can be tied by a third Te which is not bound to the Ga plane and has therefore two dangling bonds in the $(0\bar{1}1)$ plane. Thus we obtained twin tetrahedral structures $\overset{Ga}{Ga}\!>$ Te-Te-Te $<\!\overset{Ga}{Ga}$. These structures are considered as stabilized and they can be duplicated several times. Now each Cd reaching the surface can tie two central Te in the $(0\bar{1}1)$ plane, driving a slight motion of the central Te with respect to bond lengths and bond angles. These tetrahedral distortions occurring during the Te relaxation affect the number of Cd that can be bound. As a result, stable clusters of atoms take form involving at most four or five Cd bound to five or six Te, as schematized in Fig. 4. At this point the multilayer growth process starts leading to (100) oriented films with the following epitaxial relations (100)CdTe$\parallel$(100)GaAs and [011]CdTe$\parallel$[011]GaAs. In an attempt to achieve a quantitative description of the clusters one can take 2.86 Å for the covalent Te-Te bond length and a value between 2.55 Å (for Ga–Te in Ga_2Te_3) and 2.81 Å (CdTe) for the Ga–Te bond. Using a value of 2.7 Å it is found that the Te plane is located at the level of the (100)As plane, i.e., at 1.41 Å up to (100)Ga initial surface with bond angles GaTeGa = 95°8 and GaTeTe = 115°. If it is assumed that the ability of the basic cell to distort is closely related to bond length variation, for instance a 5% variation, then the cluster is found to be constituted of 5 Cd and 18 Te atoms, among which only six Te are central and active in initiating the (100) multilayer growth. As soon as the second layer of Te tries to settle up, the matching of interatomic spacings along the $[0\bar{1}1]$ axis, as appeared before along the [011] direction, leads to a limitation of the number of Te that can be bound at one run. As a consequence, periodic lines of misfit dislocations extending along $[0\bar{1}1]$ and [011] directions are expected with spacings subjected to the number of Te per cluster, for instance 22.9, 27.5, and 32.1 Å for 15 Te, 18 Te, and 21 Te clusters, respectively. Such an effect has been experimentally observed and reported by Ponce *et al.*[6] They have shown, using high-resolution transmission electron microscopy, that the CdTe/GaAs interface was locally coherent and exhibits the presence of a periodic array of misfit dislocations, with dislocations running parallel to [011] and $[0\bar{1}1]$ directions along the interface and a two-dimensional periodicity of 31 Å.

Since our goal is to show how defects are created by accumulation of elastic strains, we need a more elaborate model of atomic interactions. To our knowledge, apart from "ab initio" quantum mechanical calculations - not applicable to our problem - two types of interaction models have been used.

The first is the "many body interaction potentials [6][7][8] based on Lennard-Jones type potential, and a Axilrod-Teller three body interactions. This has been used mainly to describe the structural and energetic properties of surfaces and defects in semiconductors. This type of interactions should be, in principle, associated with a MOLECULAR DYNAMICS calculation to simulate the crystal growth. But, the computation time results prohibitive. Furthermore, there is no physical basis to describe chemical bonding in semiconductors by these types of potentials : the agreement with experimental results can only be achieved by fitting a quite large set of adjustable parameters.

The second approach, developed by Chemists [9], is the MOLECULAR MECHANICS where the chemical bond is the basic interaction mode. The interaction energy is then considered as the sum of the chemical bonding terms , in accordance with crystal growth calculations, and a STRESS ENERGY related to bond lengths and bond angle variations. This approach has been applied with success to describe structural properties of molecules, but also to explain the local order in ternary compounds [10] [11] . .

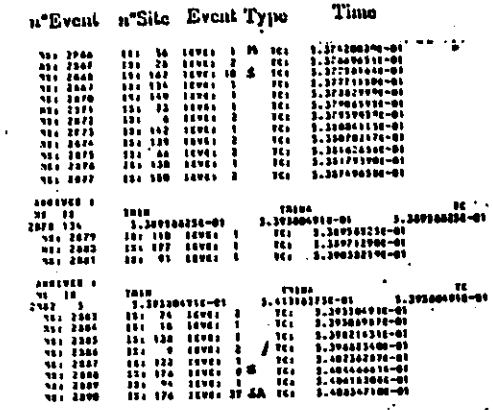

Figure 1. Typical sequence of events versus temperature. A : Arrival ; M : Migration ; S :Defect Creation ; SA :Defect Annihilation.

Since the Molecular Mechanics approach is a static one, it has been associated with a MONTE CARLO procedure to simulate dynamics of crystal growth. Following A. Madhukar [5], we assign a random time weighted by statistical thermodynamics considerations, to each possible event on the surface. However, our own contribution is that, after each event, the substrate and adsorbed atoms rearrange themselves in order to minimize the total energy of the system. A new set of possible events is then determined, and the operation is started again. At this point, local stresses on the surface may weaken the chemical bonding energy such that defects may be created. A typical sequence of events with atom inpingments, migrations, stable and unstable defect creations (creation followed by an immediate annihilation.) is illustrated in Figure 1 (30 events) ; from the whole sequence of events, the statistical distribution of different types of events as a function of temperature has been deduced (Figure 2).

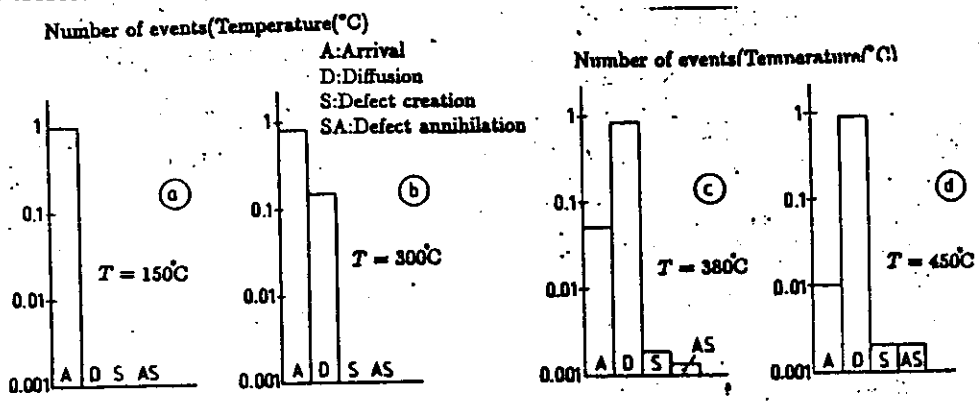

Figure 2. Statistical distribution of events as a function of temperature.
a) T = 150°C ; b) T = 300°C ; c) T = 380°C ; d) T = 450°C
A : Arrival ; D : Diffusion ; S : Defect Creation ; AS : Defect Annihilation.

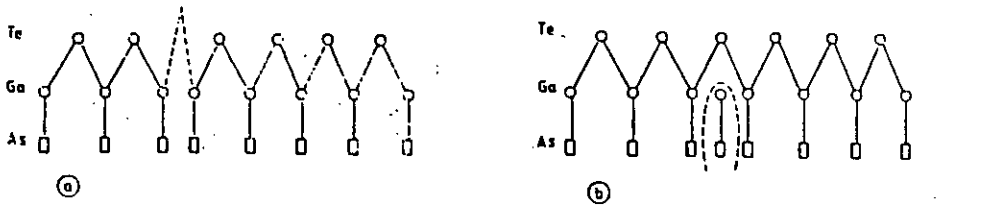

Figure 3. Schematic representation of the two punctual defects introduced in the first epi-layer. a): Te vacancy ; b) : Ga interstitial.

Interstitial defects can be only created when the total stress becomes large enough, e. when the epi-layer is near completion and in the neighborhood of a vacancy, as illustrated in Figures 4, 5, 6.

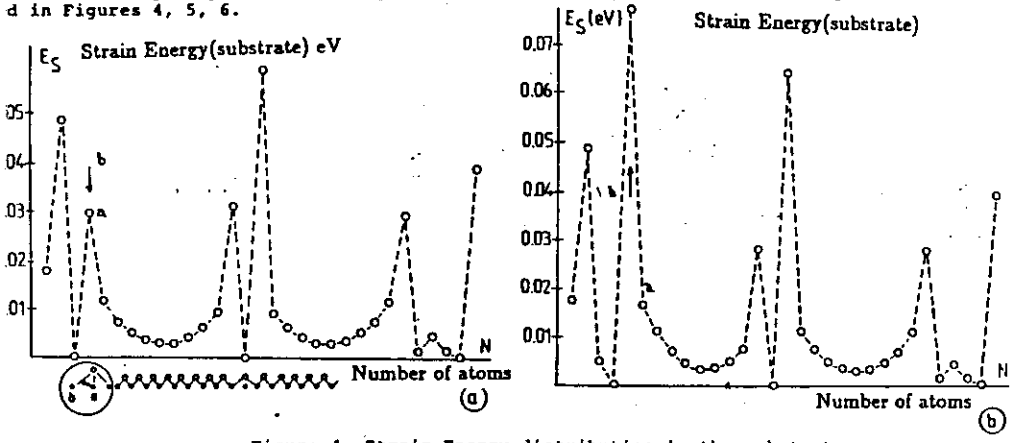

Figure 4. Strain Energy distribution in the substrate. (a) before, and (b) after creation of an unstable defect.

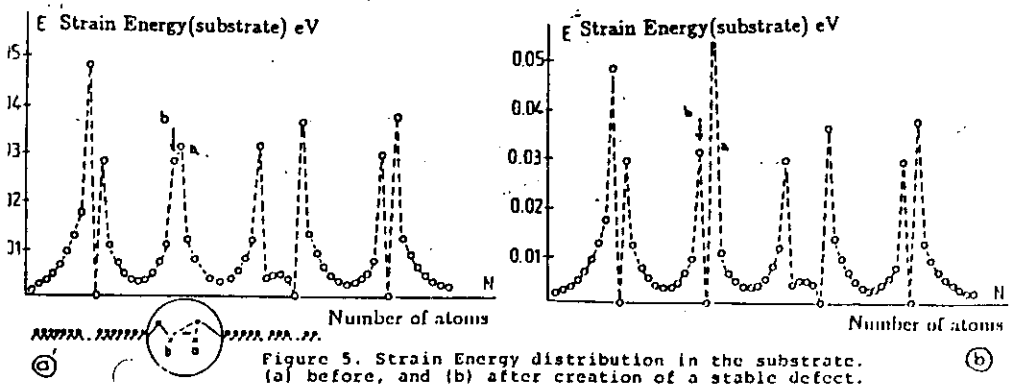

Figure 5. Strain Energy distribution in the substrate. (a) before, and (b) after creation of a stable defect.

In the simulation of the epitaxy of one monolayer on a substrate with 14.7% lattice mismatch, the epi-layer is in compression while the substrate is stretched. In our results applied to the CdTe on GaAs system, the electrostatic interactions are not considered, our first purpose being restricted to the analysis of the defect creation. Given the relative values of Young's modulus to shear modulus, it appears that bond angle variations are 20 to 50 times larger than bond length deformations. This will create an anisotropy of deformations on a <100> surface. We assume, in our B.R.M. Model, that atomic displacements are limited toward only one dimension. For computational simplification, the total energy is further developed in a second power series of the strain in the substrate. This will avoid iterative procedure in energy minimisation but includes the effect of bond length variations.

Here, only <100> growth on a <100> substrate will be considered, ruling out any trihedral configuration. The adsorbed atoms are all bonded and mobile along the 110 direction. If we deposit Te atoms on top of a defect free <100> Ga surface, two types of defects are introduced near the surface of the epi-layer (Figure 3) :

(i) The vacancies in the epi-layer which are stabilized only when an equilibrium with the second epi-layer is reached.
(ii) Ga interstitials on the substrate surface with two dangling bonds.

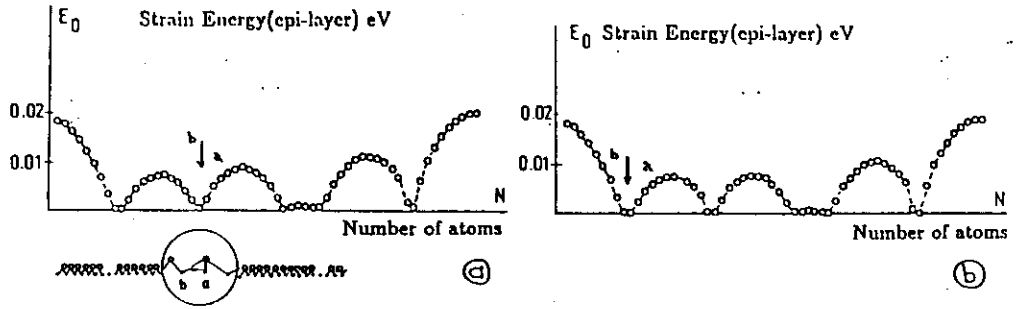

Figure 6. Strain Energy distribution in the epi-layer (a) before, and (b) after creation of a stable defect.

Interstitials are created in this example every 20 atoms, when the substrate is considered much softer than the epi-layer.This model shows that two conditions have to be fulfilled for the creation of an interstitial defect :i) high enough strain in the substrate, ii) existence of vacancies in the epi-layer.

The first condition implies that the layer is in completion, while the second is best fullfilled at low coverage. This discrepancy limits the possibility to create interstitials and explains the fact that at the stage of one monolayer, the periodicity is 20 atoms instead of seven as expected. However we can expects that -the strain increasing with the thickness of the epilayer- if the epilayer can easily exchanges atoms with the ambient or subsequent layers the number of interstitial defects would certainly increase as experimentally. observed.

Depending on local deformation of the substrate, intersititals are stable or unstable, i.e. annihilated rapidly after creation. As shown in Figure 4, the creation of an unstable defect results in an increase of the total energy while the creation of a stable defect leads to the relaxation of the energy. This relaxation occurs near the defect in the substrate (Figure 5), but far from the defect in the epi-layer (Figure 6).

In the case of rigid substrate, no. interstitial defect are observed in the first epi-layer because of the small strain in the substrate. This underlines the importance to give to the subsequent epi-layers as they will induce strain in the substrate.

The anisotropy of atomic displacement on a <100> surface leads to a periodic distribution of interstitials along the high mobility lines and a random distribution of interstitial along the low mobility lines. Since the high mobility lines are orthogonal from the first to the second epilayer, the growth of the second epilayer will certainly tend to align vacancies and interstitials already present in the first layer, to create large dislocations.

The combination of Molecular Mechanics and a Monte Carlo Method appears to be a good way to analyse and simulate heteroepitaxial growth, taking into account the strain effect on chemical bonding. The simplified version we have presented, only concerns the first deposited layer. The model allows to show the mechanism of vacancies relaxation and of interstitial creation by substrate deformation.However, the association of such defects to create dislocations can be seen only if more epi-layers are present.